Stellar Relaxation Processes Near the Galactic Massive Black Hole†

By Tal Alexander[1,2]

[1]Faculty of Physics, Weizmann Institute of Science, PO box 26, Rehovot 76100, Israel
[2]William Z. and Eda Bess Novick Career Development Chair

The massive black hole (MBH) in the Galactic Center and the stars around it form a unique stellar dynamics laboratory for studying how relaxation processes affect the distribution of stars and compact remnants and lead to close interactions between them and the MBH. Recent theoretical studies suggest that processes beyond "minimal" two-body relaxation may operate and even dominate relaxation and its consequences in the Galactic Center. I describe loss-cone refilling by massive perturbers, strong mass segregation and resonant relaxation; review observational evidence that these processes play a role in the Galactic Center; and discuss some cosmic implications for the rates of gravitational wave emission events from compact remnants inspiraling into MBHs, and the coalescence timescales of binary MBHs.

1. Introduction

The $M_\bullet \sim 4\times10^6\,M_\odot$ massive black hole (MBH) in the Galactic Center (GC) (Eisenhauer *et al.* 2005; Ghez *et al.* 2005) and the stars around it are the closest and observationally most accessible of such systems. Observations of the GC thus offer a unique opportunity to study in great detail the effects of the MBH and its extreme environment on star formation, stellar evolution and stellar dynamics, and the interactions of stars and compact remnants with the MBH.

Here the focus is stellar relaxation processes. Relaxation plays an important role in a wide range of phenomena that involve close interactions with a MBH (the "loss-cone problem", §1.1). Such processes include gravitational wave (GW) emission by compact remnants inspiraling into a MBH ("extreme-mass ratio inspiral events" (EMRIs, see review by Amaro-Seoane *et al.* 2007, tidal flares from tidal disruption events (Frank & Rees 1976), tidal capture and tidal scattering of stars (Alexander & Morris 2003; Alexander & Livio 2001), 3-body exchanges with binaries leading to the capture of stars on tight orbits around the MBH and the ejection of hyper velocity stars (HVSs) out of the galaxy (Hills 1988), the orbital decay and coalescence of a binary MBHs (and the "last parsec stalling problem", see review by Merritt & Milosavljević 2005), and perhaps also the formation of ultra-luminous X-ray sources (ULXs) in star clusters following stellar capture around an intermediate mass black hole (IMBH) (Hopman *et al.* 2004). Relaxation processes are possibly linked to the presence and properties of unusual stellar populations that are observed near MBHs, such as the central "S-star" cluster, the stellar disks in the GC (Eisenhauer *et al.* 2005; Paumard *et al.* 2006) and the stellar disk in M31 (Bender *et al.* 2005).

Dynamical relaxation by star-star interactions is inherent to the discreteness of stellar systems. In the absence of additional mechanisms to randomize stars in phase-space, standard 2-body stellar relaxation assures a minimal degree of randomization, albeit one that could be too slow to be of practical interest. This review will discuss relaxation processes beyond standard stellar relaxation, which operate on much shorter timescales, or else operate in a qualitatively different way: massive perturbers (§2), strong mass segregation (§3) and resonant relaxation (§4).

The dynamical properties of the GC, specifically its short 2-body relaxation time and high stellar density, are probably not typical of galaxies in general (§1.2). However, dynamical processes that can be probed by GC observations have implications beyond the GC. In particular, the

† Invited talk. To appear in "2007 STScI spring symposium: Black Holes", eds, M. Livio & A. M. Koekemoer, Cambridge University Press, in press.

Milky Way is the archetype of the subset of galaxies with low-mass MBHs that are key targets for planned space-borne gravitational wave detectors, such as the Laser Interferometer Space Antenna (LISA). GC studies may help understand the effect of such relaxation processes on the open questions of the cosmic EMRI event rate and the EMRI orbital characteristics.

Before turning to a discussion of the non-standard relaxation processes that are expected to operate in the GC, it is useful to briefly review the dynamics leading to close interactions with a MBH (loss-cone theory) and the dynamical conditions in the GC.

1.1. *Infall and inspiral into a MBH*

Stars can fall into the MBH either by losing orbital energy, so that the orbit shrinks down to the size of the last stable circular orbit ($r_{\rm LSCO}=3r_s$ for a non-rotating MBH, where the event horizon is at the Schwarzschild radius $r_s=2GM_\bullet/c^2$), or by losing orbital angular momentum so that the orbit becomes nearly radial and unstable (periapse $r_p<2r_s$ for a star with zero orbital energy falling into a non-rotating MBH)†. The timescale to lose energy by 2-body scattering, $T_E\equiv|E/\dot{E}|$ is of the order of the relaxation time,

$$T_E\sim T_R\sim\left(M_\bullet/M_\star\right)^2\tau_{\rm dyn}(r)/N_\star(<r)\log N_\star(<r)\,, \tag{1.1}$$

where $N_\star(<r)$ is the number of stars inside r, $\tau_{\rm dyn}(r)\sim\sqrt{r^3/GM_\bullet}$ is the dynamical time and spherical symmetry and a Keplerian velocity dispersion are assumed, $\sigma^2\sim GM_\bullet/r$. The maximal angular momentum available for an orbit with energy E is that of a circular orbit, $J_c(E)=GM_\bullet/\sqrt{2E}$ (using here the stellar dynamical sign convention $E\equiv-v^2/2-\phi(r)>0$). The timescale for losing angular momentum, $T_J\equiv|J/\dot{J}|$, can be much shorter than T_E when $J<J_c$, since

$$T_J=[J/J_c(E)]^2T_E\,. \tag{1.2}$$

As a consequence, almost all stars that reach the MBH, and are ultimately destroyed by a close interaction with it, do so by being scattered to low-J "loss-cone" orbits (near radial orbits with $J<J_{lc}\simeq\sqrt{2GM_\bullet q}$, where q is the maximal periapse required for the close interaction of interest to occur. Frank & Rees 1976; Lightman & Shapiro 1977). The rate of close interaction events, $\Gamma_{\rm lc}$, is set by the replenishment rate of stars into the loss-cone. When the replenishment mechanism is diffusion in phase space by 2-body scattering, $\Gamma_{\rm lc}\propto T_R^{-1}$, which is typically a very low rate. Close to the MBH, at high-E, where the relative size of the loss-cone in phase-space is large ($J_{lc}/J_c\propto\sqrt{qE}$), relaxation is too slow to replenish the lost stars, and the loss-cone is on average empty. Farther out, at low E, where the loss-cone is small, relaxation can replenish the lost stars, the loss-cone is full (isotropic distribution of stars) and the local replenishment rate is maximal. Nevertheless, the contribution to the total replenishment rate from the low-E, full loss-cone regions of phase-space, where the timescales are longer and the stellar densities lower, remains small compared to that from the empty loss-cone regions at high-E (Lightman & Shapiro 1977).

The observational and theoretical interest in such close interactions motivated numerous investigations of alternative efficient loss-cone replenishment mechanism, such as 2-body relaxation in non-spherically symmetric potentials (Magorrian & Tremaine 1999; Berczik *et al.* 2006), chaotic orbits in triaxial potentials (Norman & Silk 1983; Merritt & Poon 2004; Gerhard & Binney 1985; Holley-Bockelmann & Sigurdsson 2006), relaxation by massive perturbers (Zhao *et al.* 2002; Perets *et al.* 2007), resonant relaxation (Rauch & Tremaine 1996; Rauch & Ingalls 1998; Hopman & Alexander 2006*a*; Levin 2007), or perturbations by a massive accretion disk or a secondary IMBH (Polnarev & Rees 1994; Levin *et al.* 2005).

† If the stars are tidally disrupted before falling in the MBH, the relevant distance scale is the tidal disruption radius $r_t\sim R_\star(M_\bullet/M_\star)^{1/3}>r_s$ rather than the event horizon r_s.

Close interactions with a MBH fall in two dynamical categories (Alexander & Hopman 2003): infall processes, such as tidal disruption, where the star is destroyed promptly on its first close encounter with the MBH, and inspiral processes, such as GW EMRI events, where multiple consecutive close encounters are required for the orbit to gradually decay. The infall takes about an orbital period, the time to fall from the point of deflection to the center, whereas the inspiral process takes much longer, depending on the energy extraction efficiency of the dissipational mechanism involved (for example GW emission, tidal heating or drag against a massive accretion disk). In most cases the dissipated energy is a steeply decreasing function of the the periapse‡ and so the inspiral time scales with the number of periapse passages, and hence with the initial orbital period.

An infall or inspiral event can occur only if the star, once deflected into the loss-cone, avoids being re-scattered out of it (and in the case of inspiral, also avoids being scattered directly into the MBH). Because inspiral processes are slow, stars can avoid re-scattering, complete the inspiral and decay to an interesting, very short period orbit with high emitted dissipative power, only if they are deflected into the loss cone from an initially short period orbit, with $E > E_{\rm crit}$. Figure (1) shows a schematic description of the phase-space evolution of infalling and inspiraling stars, and the emergence of a critical energy scale. For inspiral by GW emission into a $M_\bullet \sim O(10^6\,M_\odot)$ MBH, $E_{\rm crit}$ corresponds to an initial distance scale of $r_{\rm crit} \sim 0.01$ pc (the *ansatz* $r \leftrightarrow E = GM_\bullet/2a$, is assumed here, where a is the Keplerian semi-major axis). The EMRI event rate is then approximately (Hopman & Alexander 2005)

$$\Gamma_{\rm lc} \sim N_{\rm GW}(<r_{\rm crit})/T_R(r_{\rm crit}) \propto N_{\rm GW}(<r_{\rm crit})N_\star(<r_{\rm crit})/\tau_{\rm dyn}(r_{\rm crit})\,, \qquad (1.3)$$

where $N_{\rm GW}(<r)$ is the number of potential GW sources (compact remnants) within distance r of the MBH. A critical energy can be similarly defined for infall processes. Because infall is much faster than inspiral, $E_{\rm crit}$ is much lower ($r_{\rm crit}$ much larger). For example, the critical radius for tidal disruption in the GC is $r_{\rm crit} \sim$ few pc (Lightman & Shapiro 1977; Syer & Ulmer 1999; Magorrian & Tremaine 1999). Most of the stars that infall or inspiral originate near $r_{\rm crit}$.

Equation (1.3) shows that the degree of central concentration of compact remnants strongly affects the EMRI event rate. Mass segregation therefore substantially increases the predicted EMRI event rate from inspiraling $\mathcal{O}(10\,M_\odot)$ stellar black holes (SBHs), which are the most massive, long-lived objects in the population (Hopman & Alexander 2006*b*; §3). Similarly, the capture of compact remnants very near the MBH by 3-body exchanges between the MBH and binaries (§2) can also strongly affect the EMRI rate (Perets, Hopman & Alexander, 2007, in prep.). The dependence of $\Gamma_{\rm lc}$ on T_R is not trivial, since $r_{\rm crit}$ itself depends on T_R: the shorter the relaxation time, the faster stars are scattered into the loss-cone, but also out of it. Detailed analysis shows that the two effects cancel out for $n_\star \propto r^{-3/2}$ stellar cusps. Since in most galactic nuclei the logarithmic slope of the density profile is not much different from $-3/2$, the EMRI rate is expected to be roughly independent of the relaxation time (Hopman & Alexander 2005). It should be emphasized that this result applies only to 2-body relaxation, and needs to be re-examined if other loss-cone replenishment mechanisms dominate the dynamics.

1.2. *The dynamical state of the stellar system around the Galactic MBH*

The stellar system around the Galactic MBH is expected to be in a state of dynamical relaxation in a high density cusp. This is a direct consequence of the low mass of the Galactic MBH and of the $M_\bullet/\sigma$ relation, the tight observed correlation between the mass of central MBHs and the typical velocity dispersion in the bulges of their host galaxies, $M_\bullet \propto \sigma^\beta$, where $4 \lesssim \beta \lesssim 5$ (Ferrarese & Merritt 2000; Gebhardt *et al.* 2000). $\beta = 4$ is assumed here for simplicity; the conclusions below are reinforced if $\beta > 4$.

‡ E.g. the GW energy emitted per orbit scales as $\Delta E \propto (M_\star c^2/M_\bullet)(r_p/r_s)^{-7/2}$ (Peters 1964).

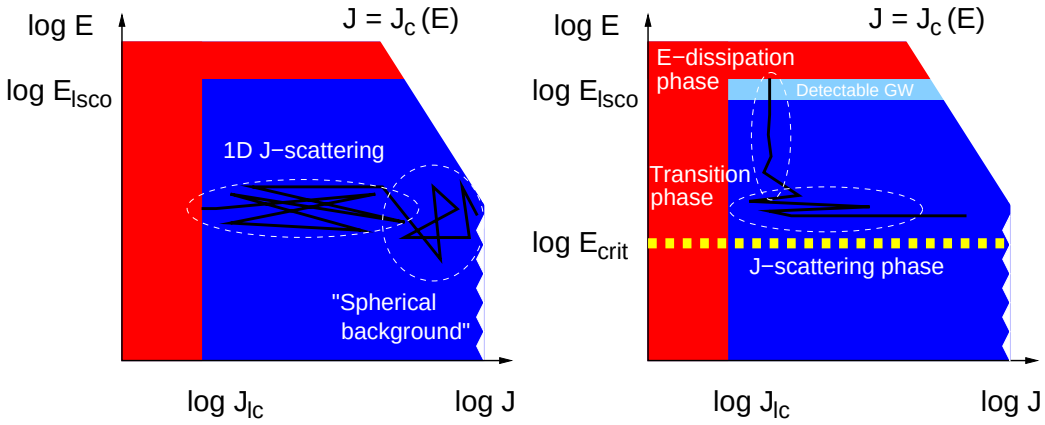

FIGURE 1. A schematic representation of the phase-space $(\log E, \log J)$ trajectories leading a star to the MBH. Each segment of the random-walk trajectory represents the change in the phase coordinates over some fixed time step Δt. The shaded areas on top ($E > E_{\rm LSCO}$) and on the left ($J < J_{\rm lc}$) are regions of phase space where no stable orbits exist. The diagonal boundary on the right is s the maximal angular momentum $J_c(E)$. Left: Infall without dissipation. A star with initially high J is scattered with roughly equal relative magnitude in E and J. Eventually a random kick will send it to a low-J orbit, where J-scattering is much faster than E-scattering, making it plunge directly into the MBH. Right: Inspiral with dissipation. Energy dissipation by the emission of GW can lead to very rapid orbital decay on low-J orbits, faster than the mean time between scattering events, thus enabling the star to reach a short-period orbit with detectable GW emission (narrow horizontal shaded strip on top). Statistically, nearly all stars with initial energy $E > E_{\rm crit}$ will ultimately inspiral into the MBH, while nearly all stars with $E < E_{\rm crit}$ will ultimately plunge into the MBH, following a trajectory similar to the one depicted in the left panel.

The MBH radius of dynamical influence is conventionally defined as $r_h \sim GM_\bullet/\sigma^2 \propto M_\bullet^{1/2}$. The mass in stars within the radius of influence is of the order of the mass of the MBH, so their number is $N_h \sim M_\bullet/M_\star$, where $M_\star$ is the mean stellar mass, and the average stellar density within r_h is $\bar{n}_h \sim N_h/r_h^3$. The two-body relaxation time at r_h is $T_R \sim (M_\bullet/M_\star)^2\, \tau_h/N_h$. It then follows that $T_R \propto M_\bullet^{5/4}$ and $\bar{n}_h \propto M_\bullet^{-1/2}$. Evaluated for the Galactic MBH, $T_R \sim \mathcal{O}(1\,{\rm Gyr}) < t_H$ (the Hubble time) and $\bar{n}_h \sim \mathcal{O}(10^5\,{\rm pc}^{-3})$. The short relaxation time implies that the system will return to its relaxed steady state following a major perturbation, such as a merger with a second MBH (Merritt & Szell 2006; Merritt *et al.* 2007). Note that $T_R > t_h$ for a MBH only a few times more massive than the Galactic MBH. The GC is thus a member of a relatively small subset of galaxies with high-density relaxed stellar cusps.

A relaxed stellar system is expected to settle into a power-law cusp distribution, $n_\star \propto r^{-\alpha}$, (§3). The high stellar density in a steeply rising cusp allows star-star and star-MBH interactions to become frequent enough to be dynamically relevant and observationally interesting (Eq. 1.3). For example, the rates of both tidal disruption events (Wang & Merritt 2004) and EMRI inspiral events (Hopman & Alexander 2005) scale inversely with the MBH mass, $\Gamma \propto N_h/T_R \propto M_\bullet^{-1/4}$.

2. Massive perturbers

2.1. *Massive perturbers and the loss-cone*

The relaxation time (Eq. 1.1) is proportional to $(M_\star^2 n_\star)^{-1}$. This can be readily understood by considering the "$\Gamma \sim nv\Sigma$" collision rate between stars of mass $M_\star$ and mean space density in volume V, $n_\star = N_\star/V$, where the cross-section $\Sigma \sim \pi r_c^2$ is evaluated for collisions at the capture radius $r_c = 2GM_\star/v^2$, the minimal radius for a soft encounter with a typical velocity v. The rate of scattering by stars is then $\Gamma_\star \sim n_\star M_\star^2/v^3 \sim T_R^{-1}$ (integration over all collision radii

increases the rate only by a logarithmic Coulomb factor). When the system also contains a few very massive objects such as giant molecular clouds (GMCs), stellar clusters, or IMBHs (if such exist), these massive perturbers (MPs) of mass $M_p \gg M_\star$ and space density $n_p = N_p/V \ll n_\star$ will scatter stars at the capture radius $r_c = G(M_\star + M_p)/v^2$ at a rate of $\Gamma_p \sim n_p(M_\star + M_p)^2/v^3 \sim n_p M_p^2/v^3$. MPs could well dominate the relaxation even if they are very rare, as long as

$$\mu_2 \equiv M_p^2 N_p / M_\star^2 N_\star > 1 \,. \tag{2.1}$$

Efficient relaxation by MPs was first suggested by Spitzer & Schwarzschild (1951, 1953) to explain stellar velocities in the Galactic disk. Its relevance for replenishing the loss-cone was subsequently investigated in the context of Solar system dynamics for the scattering of Oort cloud comets to the Sun (Hills 1981; Bailey 1983), and more recently as a mechanism for establishing the $M_\bullet/\sigma$ correlation by fast accretion of stars and dark matter (Zhao *et al.* 2002). Here the focus is on the consequences of MPs for the replenishment of the loss-cone, and the implications for stellar populations in the Galaxy (Perets *et al.* 2007), the coalescence of binary MBHs (Perets & Alexander 2007) and for the cosmic rates of EMRIs (Perets, Hopman & Alexander, in prep.).

Loss-cone replenishment by MPs can be described by the standard loss-cone formalism (e.g. Young 1977) with only few modifications (Perets *et al.* 2007). The large size of the MPs is taken into account by decreasing the Coulomb logarithm accordingly; the orbital averaging of phase-space diffusion due to scattering by stars is done incoherently (sum of squares), while for rare MPs, where there may be on average less than one scattering events per orbital period, the averaging is done coherently (square of sums).

The relative contributions of relaxation by stars and relaxation by MPs to the total loss-cone replenishment rate depend on the size of $r_{\rm crit}$ relative to the spatial distribution of the MPs ($r_{\rm crit}$ increases with the loss-cone size, and in the case of inspiral also with the efficiency of the dissipative process). MPs are extended objects, which cannot survive in the strong tidal field of the MBH (IMBHs could be the one exception). Generally, MPs in galactic centers could also be affected by an intense central radiation field, whether the AGN's or the stars', or by outflows associated with accretion on a MBH. These processes introduce an inner cutoff $r_{\rm MP}$ to the MP distribution. A plausible estimate is $r_{\rm MP} \gtrsim \mathcal{O}(r_h)$. This is the case in the GC, where the clumpy circumnuclear gas ring lies outside the central 1.5 pc, on a scale comparable to r_h. The event rates of processes such as tidal disruption of single stars ($r_{\rm crit} \sim r_h$) or GW EMRI ($r_{\rm crit} \ll r_h$), where stellar relaxation by itself efficiently fills the loss-cone at $r_{\rm crit} < r < r_{\rm MP}$, will not be much enhanced by additional relaxation due to MPs (the stellar distribution function (DF) cannot be more random than isotropic). In contrast, the event rates of processes whose loss-cone is large, and which would have remained empty beyond $r_{\rm MP}$ in the absence of MPs, can be increased by orders of magnitude by the presence of MPs. Most of the enhancement is due to MPs near $r_{\rm MP}$ (Perets *et al.* 2007).

Here we consider two processes with large loss-cones, where MPs play an important role: the tidal disruption of stellar binaries of total mass M_{12} and semi-major axis a_{12} that interact with the MBH at a distance $r_p < r_t \sim a_{12}(M_\bullet/M_{12})^{1/3}$, leading to the capture of one star around the MBH and the ejection of the other as a HVS (Hills 1988), and the orbital decay of a binary MBH of total mass M_{12}, mass ratio $M_2/M_1 = Q < 1$ and semi-major axis a_{12} by interactions with stars at a distance $r_p \lesssim \mathcal{O}(a_{12})$ (the "slingshot effect") (Begelman *et al.* 1980).

2.2. *Massive perturbers in the Galactic Center*

MPs in the GC include GMCs, stellar clusters and possibly IMBHs, if these exist. Direct observational evidence (Fig. 2) indicates that the dominant MPs on the $r \sim$ 5–100 pc scale are $\mathcal{O}(100)$ GMCs in the mass range 10^4–$10^8\,M_\odot$, with rms mass of $\sim 10^7\,M_\odot$ and a typical size of $R_p \sim 5$ pc (the quoted range includes an order of magnitude uncertainty in the mass determina-

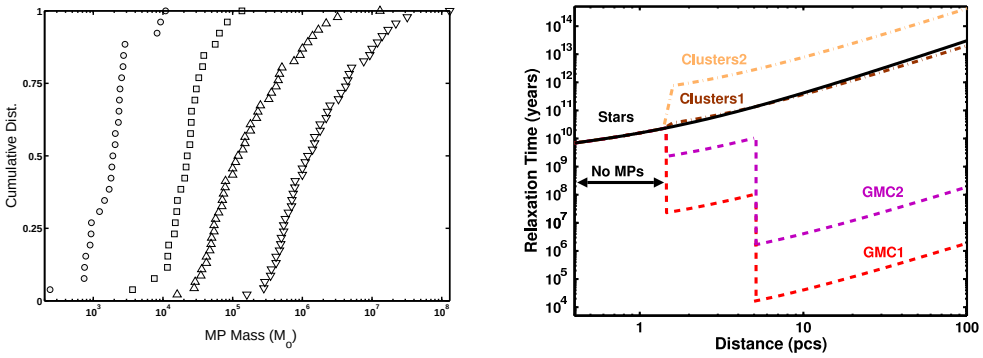

FIGURE 2. The observed MPs in the GC and their effect on the relaxation time. Left: The observed mass function of molecular cloud massive perturbers in the GC (adapted from Perets *et al.* (2007) with permission from the *Astrophysical Journal*). Lower (○) and upper (virial) (□) mass estimates for the molecular clumps in the inner ~ 5 pc, based on the molecular line observations of Christopher *et al.* (2005), and lower (△) and upper (virial) (▽) mass estimates for the GMCs in the inner ~ 100 pc of the Galaxy, based on the molecular line observations of Oka *et al.* (2001). Right: The relaxation time as function of distance from the Galactic MBH due to stars alone, the upper (GMC1) and lower (GMC2) mass estimates of the molecular clumps and GMCs and due to upper (Clusters1) and lower (Clusters2) estimates on the number and masses of stellar clusters. The sharp transitions at $r = 1.5$ and 5 pc are artifacts of the non-continuous MP distribution assumed here. GMCs dominate the relaxation in the GC.

tion), (Oka *et al.* 2001; Güsten & Philipp 2004), and on the $r \sim 1.5$-5 pc scale, $\mathcal{O}(10)$ molecular clumps† with masses in the range 10^3–$10^5\,M_\odot$, with rms mass of $\sim 10^4\,M_\odot$ and a typical size of $R_p \sim 0.25$ pc (Christopher *et al.* 2005). The ~ 10 observed stellar clusters (Figer *et al.* 1999; Borissova *et al.* 2005) may compete with stellar relaxation (Perets & Alexander 2007). Compared to the $\sim 2\times10^8 \sim 1\,M_\odot$ stars in the central 100 pc (Figer *et al.* 2004), the GMCs are expected to decrease the relaxation time by a factor $\mu_2 \sim 50$–5×10^7 (Eq. 2.1). Figure (2) shows a more detailed estimate of the local relaxation time for the various molecular cloud models, taking into account, among other considerations, the Coulomb factors. The relaxation time is indeed substantially decreased, by factors of $10 - 10^7$ relative to that by stars alone, depending on distance from the center, and on the GMC mass estimates. If IMBHs do exist, then the effects of accelerated relaxation will be even stronger than predicted here, and probably extend all the way to the center.

2.3. *Galactic and cosmic implications*

With stellar relaxation alone, the empty loss-cone region of MBH-binary interactions is large ($r_t \propto a_{12}$) and extends out to > 100 pc. However, the MPs that exist in the Galaxy on that scale accelerate relaxation, efficiently fill the loss-cone, and thus increase the binary disruption rate by several orders of magnitude, making binary disruptions dynamically and observationally relevant (Perets *et al.* 2007). Such events, which result in the energetic ejection of one star, and the capture of the other on a close orbit around the MBH, have various possible implications. Disruptions of binaries by the Galactic MBH (Hills 1988; Yu & Tremaine

† The division of a quasi-continuous medium into individual clouds is somewhat arbitrary, since several sub-clumps can be identified as a single cloud, depending on the spatial resolution of the observations and the adopted definition of a cloud. For a fixed total MP mass, $M = M_p N_p$ within a region of size r, the relaxation time scales with N_p as $T_R \propto (M_p^2 N_p)^{-1} = M^{-2} N_p$; the more massive and less numerous the clouds, the shorter T_R. The value of T_R thus depends on the way clouds are counted. Obviously, the statistical treatment of relaxation is valid only for $N_p \gg 1$ and $R_p \ll r$.

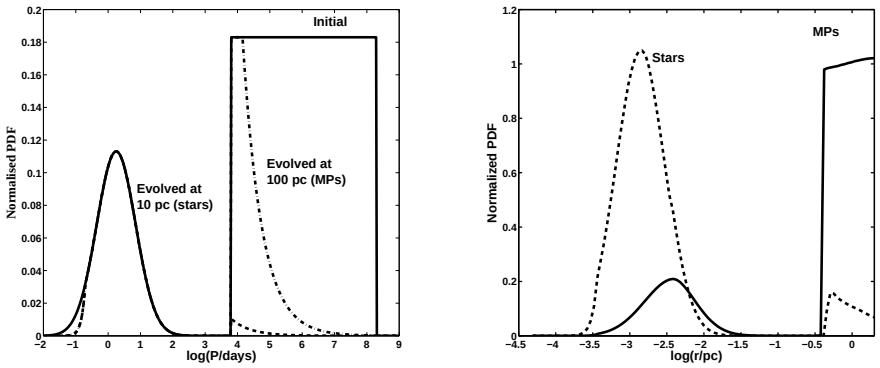

FIGURE 3. A schematic representation of the mapping of the initial binary period distribution to the semi–major axis of the tidally captured star. Left: The bimodal initial period distribution for old white dwarf / main sequence binaries (adapted from Willems & Kolb 2004), and its subsequent evolution due to GW coalescence (for the shortest periods) and to slow evaporation by field stars at 100 pc and faster evaporation at 10 pc. Right: the resulting semi-major axis distribution of the captured stars, due to scattering by stars, which occurs on the $\mathcal{O}(10\,\mathrm{pc})$ scale, and due to scattering by MPs, which occurs on the $\mathcal{O}(100\,\mathrm{pc})$ scale.

2003; Gualandris *et al.* 2005; Bromley *et al.* 2006) were suggested to be the origin of the hypervelocity B-stars‡ ($v \gtrsim 500\,\mathrm{km\,s^{-1}}$), observed tens of kpc away from the GC (Hirsch *et al.* 2005; Brown *et al.* 2005; Edelmann *et al.* 2005; Brown *et al.* 2006*a*), and the origin of the puzzling "S-stars" (Gould & Quillen 2003; Ginsburg & Loeb 2006), a cluster of $\sim$ 10–30 main-sequence B-stars ($4\,M_\odot \lesssim M_\star \lesssim 15\,M_\odot$, main sequence lifespan $t_\star \sim$ few $\times\, 10^7$–few $\times\, 10^8$ yr) on random tight orbits around the MBH in the central few $\times\, 0.01$ pc (Eisenhauer *et al.* 2005; Ghez *et al.* 2005). Compact objects captured this way could eventually become zero-eccentricity GW sources (Miller *et al.* 2005), in contrast to high-eccentricity sources typical of single-star inspiral (Hopman & Alexander 2005). These two classes of sources are expected to emit very different gravitational wave-forms.

Dynamical arguments and simulations show that on average, ~ 0.75 of MBH-binary encounters lead to capture, and that the mean semi-major axis of the captured star is related to that of the original binary by (Hills 1988, 1991)

$$\langle a \rangle \sim (M_\bullet/M_{12})^{2/3}\, a_{12}\,, \tag{2.2}$$

which implies a very high initial eccentricity, $1-e = r_t/\langle a\rangle = (M_{12}/M_\bullet)^{1/3} \sim \mathcal{O}(0.01)$. The tidal capture process can be viewed as a mapping between the properties of field binaries far from the MBH, and the orbital properties of the captured stars: wide binaries result in wide captured orbits, and vice versa (Fig. 3). The mean velocity of the ejected star at infinity (neglecting the galactic potential) is

$$\left\langle v_\infty^2 \right\rangle \sim \sqrt{2} G M_{12}^{2/3} M_\bullet^{1/3}/a_{12}\,. \tag{2.3}$$

This translates, for example, to $v_\infty \sim 2000\,\mathrm{km\,s^{-1}}$ for a $2\times 4\,M_\odot$ B-star binary with $a_{12} = 0.2$ AU, well above the escape velocity from the Galaxy.

Of particular interest is the connection between the HVSs and the S-stars that is implied by the binary tidal disruption scenario. The stellar binary mass ratio distribution is peaked around ~ 1 (Duquennoy & Mayor 1991; Kobulnicky *et al.* 2006), and so the observed similarity in the spectral type of the S-stars and HVSs is consistent with this scenario. Figure (4) shows an estimate of

‡ HVS candidates are chosen for spectroscopy by color, to maximize the contrast against the halo population, and so are pre-selected to have B-type spectra (e.g. Brown *et al.* 2006*b*).

the number of tidally captured S-stars for different MP populations (Perets *et al.* 2007), based on the observed orbital properties of young massive binaries ($a \sim 0.20^{+0.60}_{-0.15}$ AU) and their fraction among young massive stars in the field ($f_2 \sim 0.75$) (Kobulnicky *et al.* 2006), and on a model for the stellar density distribution in the inner ~ 100 pc of the Galaxy (isothermal, normalized by the observations of Genzel *et al.* 2003) and a mass function model (continuous star formation with a universal IMF, Figer *et al.* 2004, see also Fig. 6). The typical binary was modeled as a $2 \times 7.5\,M_\odot$ binary (main sequence B-stars with a lifespan of $t_\star \sim 5 \times 10^7$ yr). Dynamical evaporation is negligible for such short-lived binaries. The steady state number of captured S-stars is then $\langle N_\star \rangle = \Gamma_{lc} t_\star$. Figure (4) shows that with stellar relaxation alone, tidal capture cannot explain the S-star population. However, relaxation by GMCs is consistent with the observed number of S-stars, as well as with the spatial extent of the cluster of ~ 0.04 pc, which reflects the hardness of young massive binaries in the field (Eq. 2.2). It is also consistent with the fact that the S-cluster does not include any star earlier then O8V/B0V. Such short-lived binaries are very rare in the field, and their mean number in the S-cluster is predicted to be $\langle N_\star \rangle < 1$.

The MP-induced binary tidal disruption scenario also predicts that there should be 10–50 hyper-velocity $\sim 4\,M_\odot$ B-stars at distances between 20 and 120 kpc from the GC. This is consistent with the total number of 43 ± 31 extrapolated by Brown *et al.* (2006*a*), based on the HVSs detected at these distances in their field of search. The tidal disruption scenario predicts an isotropic distribution of HVSs around the GC, and a random ejection history, in contrast to models where the ejection is related to a discrete binary MBH merger event (Yu & Tremaine 2003; Haardt *et al.* 2006; Baumgardt *et al.* 2006; Levin 2006). The HVSs observed to date are consistent with an isotropic HVS distribution uniformly distributed in ejection time (Brown *et al.* 2006*a*) and thus support the tidal disruption scenario.

The tidal disruption scenario can naturally explain many of the properties of the S-stars and HVSs, but it has two potential flaws. (1) The predicted high eccentricities of the captured stars are larger than those observed for a few of the S-stars ($e \sim 0.4$, Eisenhauer *et al.* 2005). However, the low observed eccentricities are expected to evolve after the capture by rapid resonant relaxation (§4). (2) The lifespan of the most massive and shortest lived S-stars ($t_\star \sim 2 \times 10^7$ yr) is shorter by a factor $\lesssim 10$ than the MP-accelerated relaxation time in the inner ~ 5 pc (Fig. 2), where a substantial fraction of the binaries are scattered from. Thus if a binary in those regions starts on a near-circular orbit, MP-induced relaxation is not fast enough to scatter it to a $J < J_{lc}$ orbit (Eq. 1.2) within its lifetime. However, as the timescale discrepancy is not large, and as it affects only the most massive binaries in the central few pc, where the determination of T_R is ambiguous (see footnote on page 6), this does not appear to be a fatal flaw of this scenario. It does however highlight the importance of observationally quantifying the relaxation time in the GC and the distribution and properties of the field binaries.

Low-mass binaries are also deflected to the MBH by MPs and tidally disrupted at rates as high as $\sim 10^{-4}\,\mathrm{yr}^{-1}$ (Perets *et al.* 2007). Neither the faint captured low-mass stars nor the late-type HVSs are detectable at this time. However, the captured stars affect the inner cusp dynamics in a way that may have implications for cosmic GW EMRI events. Binary disruption is effectively a local "source term" that modifies the flow of stars in phase space (cf Eq. 3.3), setting a diverging flow into the MBH and away from it, which modifies the steady state spatial distribution. Detailed calculations, which take into account the period distribution of low-mass binaries and the effects of binary evaporation, indicate that MP-induced tidal captures of white dwarfs close to the MBH efficiently competes against mass-segregation, which tends to lower the density of the low-mass white dwarfs there and raise the density of massive stellar BHs (§3, Fig. 8). As a result, the cosmic rate of GW EMRI events involving white dwarfs is predicted to be at least comparable to that involving stellar BHs (Perets et al. 2007, in prep.).

The proximity of the GC allows GW bursts from the fly-by of stars near the MBH to be detected (Rubbo *et al.* 2006). MP-induced tidal binary disruptions increase the stellar density close

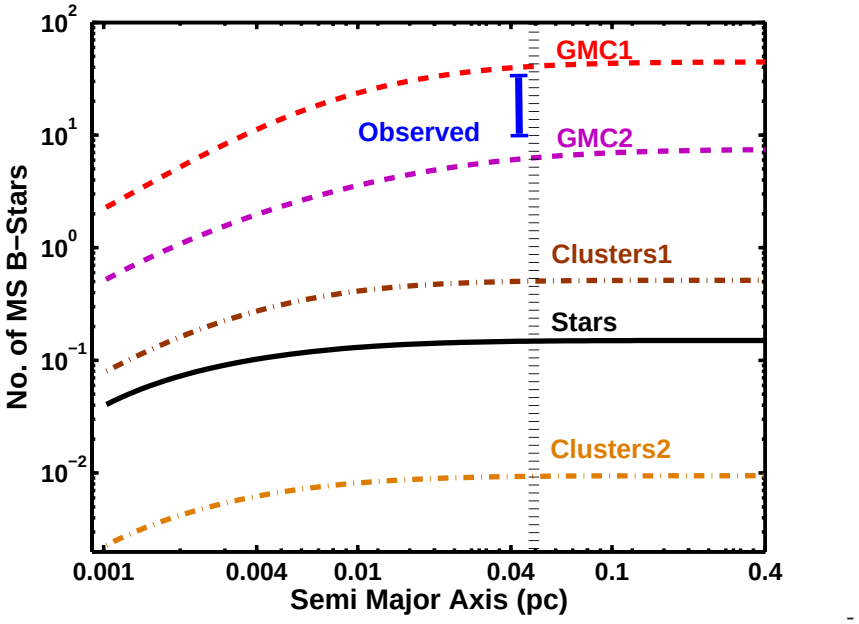

FIGURE 4. A comparison between the cumulative number of S-stars (main sequence B stars) observed orbiting the Galactic MBH on randomly oriented orbits (vertical bar), and the predicted number captured by 3-body tidal interactions of the MBH with binaries deflected to the center by massive perturbers, for different massive perturbers models (Perets *et al.* 2007). The observed extent of the S-star cluster is indicated by the vertical hashed line.

to the MBH and therefore the rate of GW bursts increases significantly. In particular, the rate of GW bursts from white dwarfs increases from $\sim 0.1\,\mathrm{yr}^{-1}$ (Hopman *et al.* 2007) to a detectable rate of $\sim 2\,\mathrm{yr}^{-1}$ (Perets et al. 2007, in prep.).

Binary MBHs form in the aftermath of galactic mergers, when the two MBHs sink by dynamical friction to the center of the merged galaxy. Once the binary hardens, the orbital decay continues by 3-body interactions with stars that are deflected to the center and extract energy from the binary, until the orbit becomes tight enough for efficient GW emission, which rapidly leads to coalescence. Simulations show that when the loss-cone is replenished by stellar relaxation alone, the interaction rate is too slow for the binary MBH to coalesce within a Hubble time (e.g. Berczik *et al.* 2005; see review by Merritt & Milosavljević 2005; Fig. 5). This "last parsec stalling problem" appears to contradict the circumstantial evidence that most galactic nuclei contain only a single MBH (Berczik *et al.* 2006; Merritt & Milosavljević 2005), and furthermore implies few such very strong GW sources for LISA. One route† for resolving the stalling problem is by accelerated MP-induced loss-cone replenishment (Perets & Alexander 2007)

Figure (5) shows the time to coalescence, as function of the binary MBH mass, for different merger and MP scenarios, based on a combination of extrapolation of the Galactic MP population to early type galaxies, on extra-galactic observations of molecular gas in galactic centers, and on results from galactic merger simulations. The results show that MPs allow binary MBHs in gas-rich galaxies to coalesce within a Hubble time over nearly the entire range of M_{12}. The situation with respect to gas-poor galaxies is less clear, since it is harder to model reliably the MPs there

† Other possible routes are by interactions with gas in "wet mergers" (Ivanov *et al.* 1999; Escala *et al.* 2005; Dotti *et al.* 2007), by interactions with a third MBH (Makino & Ebisuzaki 1994; Blaes *et al.* 2002; Iwasawa *et al.* 2006), or by accelerated loss-cone replenishment in a non-axisymmetric potential, (Yu 2002; Berczik *et al.* 2006), or in a steep cusp (Zier 2006).

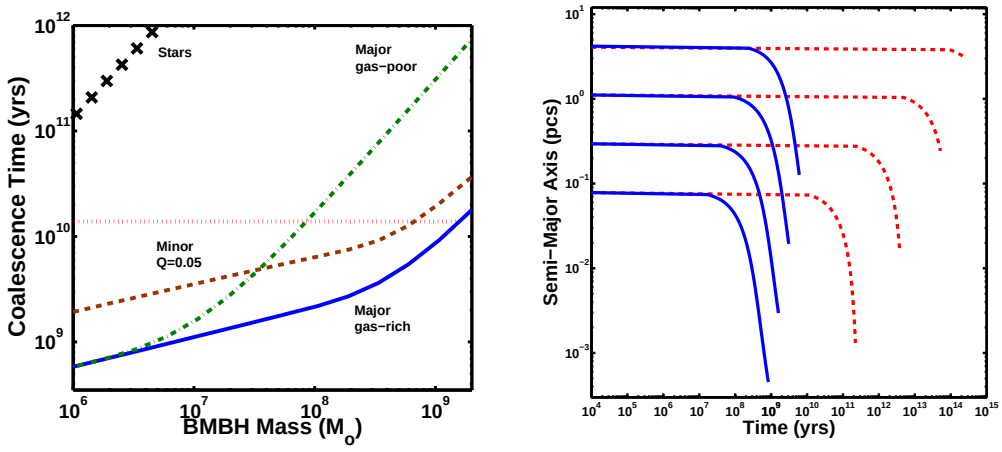

FIGURE 5. Accelerated binary MBH mergers in the presence of MPs (Perets & Alexander 2007). Left: The time to coalescence as function of binary MBH mass, for different merger scenarios distinguished by the mass ratio Q between the two MBHs and the MP contents of host galaxies. The age of the universe is indicated by the dotted horizontal line. Stellar relaxation alone cannot supply a high enough rate of stars for the slingshot mechanism to complete the merger within a Hubble time. However, in minor mergers ($Q=0.05$) major gas-rich mergers ($Q=1$) with MPs merger is possible within a Hubble time for all but the most massive MBHs. Right: The evolution of the binary MBH semi-major axis as function of time for major mergers ($Q=1$) in the presence of MPs (solid line) and stellar relaxation alone (dashed line), for binary MBH masses of 10^6, 10^7, 10^8 and 10^9 $M_\odot$ (from bottom up).

(probably clusters rather than GMCs). However, even for such galaxies, MPs allow coalescence within a Hubble time up to masses of $M_{12} \lesssim 10^8\, M_\odot$.

Efficient binary MBH coalescence by MPs has various implications. It increases the cosmic rate of GW events from MBH-MBH mergers, it increase the "mass deficit" in the galactic core (the stellar mass ejected from the core by the slingshot effect) (Milosavljević *et al.* 2002; Ravindranath *et al.* 2002; Graham 2004; Ferrarese *et al.* 2006), it leads to the ejection of hyper-velocity stars to the inter-galactic space, but it suppress the formation of triple MBH systems and the ejection of MBHs into intergalactic space (Saslaw *et al.* 1974; Blaes *et al.* 2002; Hoffman & Loeb 2007; Iwasawa *et al.* 2006).

3. Strong mass segregation

3.1. *The Bahcall-Wolf solution of moderate mass-segregation*

The 2-body relaxation timescale around the Galactic MBH, $T_R \sim \mathcal{O}(1\,\mathrm{Gyr})$, is short enough for the old stellar population there to relax to a universal steady-state configuration, independently of the initial conditions. This configuration was investigated by Bahcall & Wolf (1976, 1977). The Bahcall-Wolf solution predicts that in the Keplerian potential near a MBH, stars of mass $M_\star$ in a multi-mass population ,$M_1 < M_\star < M_2$, have a DF that is approximately a power-law of the specific orbital energy ϵ, $f_M(\epsilon) \propto \epsilon^{p_M}$, where $p_M \propto M_\star$ with a proportionality constant $p_M/M_\star \simeq 1/(4M_2)$. In a Keplerian potential, this DF corresponds to a density cusp $n_M(r) \propto r^{-\alpha_M}$, where $\alpha_M = 3/2 + p_M$. Elementary considerations show that $\alpha = 7/4$ ($p = 1/4$) for a single mass population (e.g. Binney & Tremaine 1987, § 8.4-7). This follows from the conservation of the orbital energy that is extracted from stars that are scattered into the MBH, and transferred outward by the ambient scattering stars in a steady-state, distance-independent current, $\mathrm{d}E(r)/\mathrm{d}t \sim N_\star(<r)E_\star(r)/T_R(r) \sim r^{7/2-2\alpha} = \mathrm{const}$ (using the relations $N_\star(<r) \propto r^{3-\alpha}$,

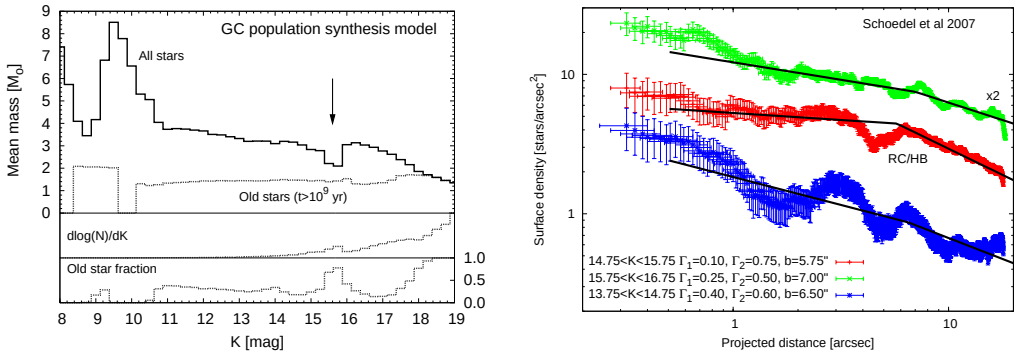

FIGURE 6. Left: A theoretical population model for the central few pc of the GC (Alexander & Sternberg 1999; Alexander 2005), assuming continuous star formation over the past 10 Gyr (Figer *et al.* 2004) with a "universal" IMF (Miller & Scalo 1979). Bottom panel: The fraction of old stars (defined here as stars with main-sequence lifespan of > 1 Gyr) in the population, as function of the K-band magnitude in the GC (for $DM+A_K = 17.2$ mag, Eisenhauer *et al.* 2005). Middle panel: The K-band luminosity function. Top panel: The mean mass of all stars and of the old stars only, as function of the K-band magnitude. The concentration of old Red Clump / horizontal branch giants around $K \sim 15.5$ is clearly seen as an excess in the luminosity function, as an increase the fraction of old stars and as a decrease in the mean stellar mass relative to stars both immediately brighter and fainter (Schödel *et al.* 2007). Right: The observed azimuthally-averaged stellar surface number density around the Galactic MBH as function of projected angular distance, $\Sigma(R)$ ($R = 1$" corresponds to ~ 0.04 pc in the GC) in 3 adjacent K-magnitude bins, centered around the bin associated with the Red Clump giants ($14.75 < K < 15.75$), with broken power-law fits $\Sigma \propto R^{-\Gamma}$ (Schödel *et al.* 2007, adapted with permission from *Astronomy and Astrophysics*). Top: $15.75 < K < 16.75$ (density multiplied by 2 for display purposes). Middle: $14.75 < K < 15.75$ (the Red Clump / horizontal branch range). Bottom: $13.75 < K < 14.75$.

$E_\star \sim r^{-1}$ and $T_R \propto r^{\alpha-3/2}$, §1.2). The Bahcall-Wolf solution reproduces this result for a single mass population, and predicts that it should apply also to the heaviest stars in a multi-mass population. The Bahcall-Wolf solution thus implies that at most $\Delta\alpha = 1/4$ between the lightest and heaviest stars in the population. The predicted degree of segregation is moderate.

Theoretical considerations, results from dynamical simulations and GC observations, hint that the moderate segregation solution should not and does not always hold, even in relaxed systems. As formulated, the solution depends only on the stellar masses, but not on the mass function. However, this cannot apply generally, since in the limit where the massive objects are very rare, they are expected to sink efficiently to the center by dynamical friction, and create a cusp much steeper than $\alpha = 7/4$. As shown below (§3.2), models of the present-day mass function in the central few pc of the GC suggest that the massive objects are relatively rare. Dynamical simulations of mass segregation in the GC based on such a mass function (Fig. 8) indeed show steep cusps ($\alpha > 2$) for the heaviest masses. Finally, the observed surface density distribution of GC stars in the magnitude bin $14.75 < K < 15.75$, which corresponds to the low-mass ($0.5 \lesssim M_\star \lesssim 2\,M_\odot$) Red Clump / horizontal branch giants (Fig. 6), is substantially flatter than that of the higher-mass giants ($M_\star \sim 3\,M_\odot$) that populate the adjacent bins of brighter and fainter magnitudes (Fig. 6; Schödel *et al.* 2007). The sign of this trend is as expected for mass segregation, but the size of the effect is much larger than predicted by the Bahcall-Wolf moderate segregation solution. However, it can be explained in terms of mass-segregation if $\Delta\alpha \gtrsim 1$ (Levi 2006). While none of these hints for strong mass-segregation is decisive in itself, and other explanations are possible, taken together they motivate a re-examination of the mass-segregation solution in a relaxed system.

3.2. *The relaxational self-coupling parameter*

Assume for simplicity a stellar system with a two-mass population of light stars of mass M_L, total initial number N_L and local density $n_L(r)$ and heavy stars of mass M_H, total initial number N_H and local density $n_H(r)$. The self interaction rate is then $\Gamma_{LL} \propto n_L M_L^2/v^3$ for the light stars and $\Gamma_{HH} \propto n_H M_H^2/v^3$ for the heavy stars (§2). In the limit where the heavy stars are test particles ($n_H/n_L \ll M_L^2/M_H^2$, or equivalently $\Gamma_{HH}/\Gamma_{LL} \ll 1$), the heavy stars interact mostly with the light ones, lose energy and sink to the center by dynamical friction. Conversely, in the limit $\Gamma_{HH}/\Gamma_{LL} \gg 1$, the heavy stars interact mostly with each other, effectively decouple from the light stars and establish an $\alpha = 7/4$ cusp typical of a single mass population. This suggests that the *global* relaxational self-coupling parameter (cf Eq. 2.1), defined as

$$\mu_2 \equiv N_H M_H^2 / N_L M_L^2 \,, \tag{3.1}$$

can be used to determine whether the system settles into the moderate (Bahcall-Wolf) mass-segregation solution ($\mu_2 > 1$) or the strong mass-segregation solution ($\mu_2 < 1$). This hypothesis is borne out by the numerical results presented below† (Alexander & Hopman 2007, in prep.; §3.3). For a continuous mass distribution, μ_2 can be generalized to

$$\mu_2 \equiv \int_{M_0}^{M_2} M_\star^2 (\mathrm{d}N/\mathrm{d}M_\star)\mathrm{d}M_\star \Big/ \int_{M_1}^{M_0} M_\star^2 (\mathrm{d}N/\mathrm{d}M_\star)\mathrm{d}M_\star \,, \tag{3.2}$$

the ratio between the 2nd moments of the mass distribution of the heavy ($M_\star > M_0$) and light ($M_\star < M_0$) stars, for some suitable choice of the light/heavy boundary mass M_0.

The value of μ_2 depends on the population's present-day mass function. So-called universal initial mass functions (IMFs), which extend all the way from the brown dwarf boundary $M_1 \sim 0.1\,M_\odot$ to $M_2 \gtrsim 100\,M_\odot$ (e.g. the Salpeter (1955) IMF, and its subsequent refinements, the Miller & Scalo (1979) and Kroupa (2001) IMFs), result in evolved populations, old star-bursts or continuously star forming populations, that naturally separate into two mass scales, the $\mathcal{O}(1\,M_\odot)$ scale of low-mass main-sequence dwarfs, white dwarfs and neutrons stars, and the $\mathcal{O}(10\,M_\odot)$ scale of stellar black holes, and typically have $\mu_2 < 1$ (Fig. 7). Such evolved populations are thus well-approximated by the simple 2-mass population model. In particular, the volume-averaged stellar population in the central few pc of the GC is reasonably well approximated by a 10 Gyr old, continuously star-forming population with a universal IMF‡ (Alexander & Sternberg 1999; Fig. 6). Generally, 10 Gyr old, continuously star-forming populations with a power-law IMF, $\mathrm{d}N/\mathrm{d}M_\star \propto M_\star^{-\gamma}$, have $\mu_2 < 1$ for $\gamma \gtrsim 2$, and $\mu_2 > 1$ for $\gamma \lesssim 2$. Since the critical value $\gamma = 2$ is close to the generic Salpeter index $\gamma = 2.35$, it is quite possible that both the moderate and strong segregation solutions are realized around galactic MBHs, depending on the system-to-system scatter in the IMF (and perhaps also realized in clusters around IMBHs, if such exist).

3.3. *Solutions of the Fokker-Planck energy equation*

The steady state configuration of stars around a MBH can be described in terms of the diffusion of stars in phase space, from an infinite reservoir of unbound stars with a given mass function (the host galaxy, far from the MBH), to an absorbing boundary at high energy where stars are destroyed (the MBH event horizon, tidal disruption radius, or collisional destruction radius).

† In the limit $M_H/M_L \gg 1$, it may be necessary to take explicitly into account the the dynamical friction timescale in order to obtain a more accurate segregation criterion. Here μ_2 is adopted for its simplicity.

‡ Note that recent analysis of late type giants in the GC suggests that the IMF in the inner ~ 1 pc of the GC could typically be a flat $\gamma \sim 0.85$ power-law (Maness *et al.* 2007). This would imply $\mu_2 \gg 1$ in the inner ~ 1 pc, possibly a volume-averaged $\mu_2 > 1$ in the inner few pc (the "collection basin" for stellar BHs, Miralda-Escudé & Gould 2000), and hence moderate segregation.

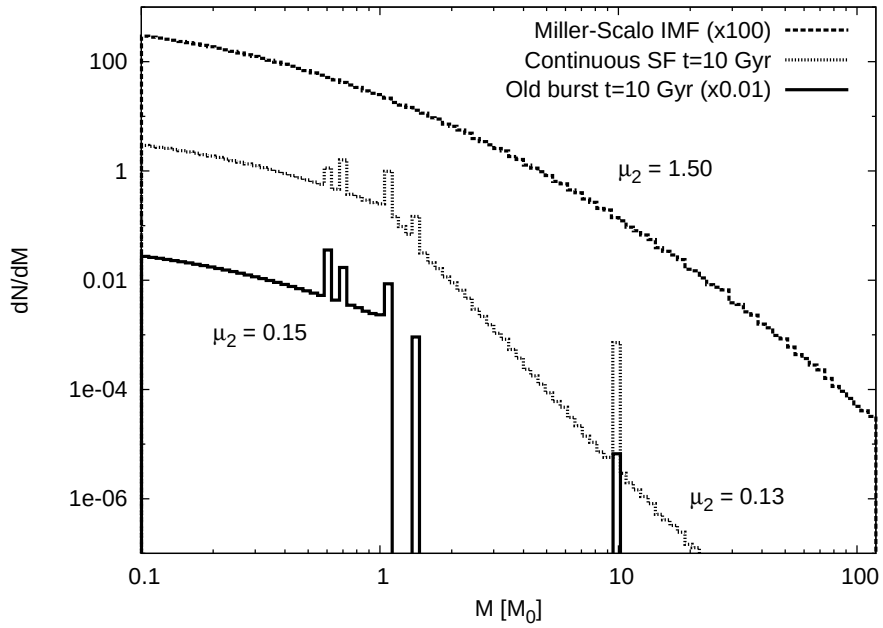

FIGURE 7. The predicted values of the global relaxational self-coupling parameter μ_2 for a "universal" Miller & Scalo (1979) IMF (top line, shifted by $\times 100$ for display purposes), an evolved mass function assuming continuous stars formation over 10 Gyr (middle line), and an evolved star formation burst 10 Gyr old (bottom line, shifted by $\times 0.01$ for display purposes) (Alexander & Hopman 2007, in prep.). The mass functions of the old populations develop excesses in the ~ 0.6–$1.4\,M_\odot$ range due to the accumulation of white dwarfs and neutron stars, and in the $\sim 10\,M_\odot$ range due to the accumulation of stellar black holes (here represented by a simplified discrete mass spectrum, see Alexander 2005, table 2.1).

Bahcall & Wolf (1976, 1977) simplified the full Fokker-Planck treatment in (E, J) phase space by integrating over J so as to reduce it to E only, by assuming a Keplerian potential, and by recasting it in the form of a particle conservation equation. In dimensionless form these can be written as (Hopman & Alexander 2006*b*)

$$\frac{\partial}{\partial\tau}g_M(x,\tau) = -x^{5/2}\frac{\partial}{\partial x}Q_M(x,\tau) - R_M(x,\tau)\,, \tag{3.3}$$

where M, x and τ are the dimensionless mass, energy, and time, respectively, g_M is the dimensionless DF, Q_M is the flow integral, which expresses the diffusion rate of stars by 2-body scattering to energies above x, and $R_M \propto g_M/T_R$ is the J-averaged effective loss-cone term. Q_M and R_M are non-linear functions of the set of DFs $\{g_M\}$. The equations are solved for $\{g_M\}$ by finite difference methods starting from an arbitrary initial DF and integrating forward in time until steady state is reached, subject to the boundary conditions that no stars exist at energies above some destruction energy x_D, $g_M(x > x_D) = 0$, and that the unbound stars are drawn from an isothermal distribution with a given mass function, $g_M(x<0) = N_M \exp(Mx)$. Bahcall & Wolf (1977) showed that the stellar space density distribution,

$$n_M(r) \propto \int_{-\infty}^{r/r_h} g_M(x)\sqrt{r/r_h - x}\mathrm{d}x\,, \tag{3.4}$$

does not depend strongly on the exact form of the loss-cone term, and proceeded to use in their mass-segregation calculations a simplified version of Eq. (3.3) by setting $R_M = 0$. This approximation can be justified by noting that while the existence of a loss-cone drastically increases

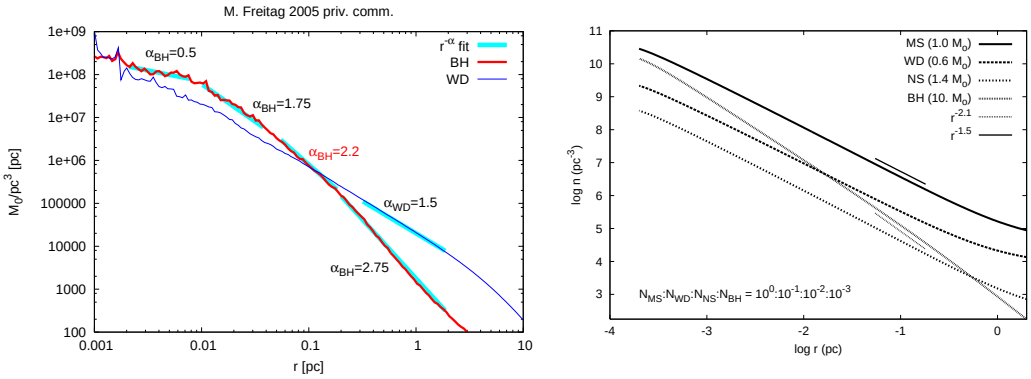

FIGURE 8. Numerical models of the mass distribution in the GC showing strong segregation. Right: The density distribution of $10\,M_\odot$ stellar BHs and $0.7\,M_\odot$ white dwarfs at 10 Gyr in an approximate model of the GC, with the evolved universal IMF of Fig. (5), derived by M. Freitag (priv. comm., reproduced here with permission. See also Freitag *et al.* 2006), using an implementation of the Hénon method (Freitag & Benz 2002). The low-mass white dwarfs settle into a $\alpha_L \simeq 1.5$ power-law cusp. The distribution of massive stellar BHs can be approximated by a piece-wise broken power-law, with $\alpha_H \sim 2.2$ at $r \sim 0.1$ pc. Left: The space density of a simplified 4-component population model for the GC, as given by the solution of the Fokker-Planck equations with a loss-cone term (adapted from Hopman & Alexander 2006*b*, with permission from the *Astrophysical Journal*). The logarithmic slope of the density cusp of the stellar BHs at $r=0.1$ pc is $\alpha\simeq 2.1$, as compared to $\alpha\simeq 1.5$ for the lighter species.

the flow rate of stars into the MBH, it typically affects only a small volume in phase space near $J \sim 0$. This translates to small changes only in the J-integrated DF $g_M(x)$, mostly for $x \to x_D$, and even smaller changes in $n_M(r)$ due to the smoothing effect of the $g_M(x) \to n_M(r)$ transformation (Eq. 3.4). Here we adopt this approximation to allow direct comparison with the Bahcall & Wolf (1977) results, after verifying that the inclusion of the loss-cone term indeed does not significantly change the derived stellar cusps (cf Fig. 8 and 9).

We calculated a suite of such Fokker-Planck mass-segregation models for 2-mass populations with different mass ratios M_H/M_L and mass functions N_H/N_L, spanning a very wide range of the global relaxational self-coupling parameter values†, $10^{-3} < \mu_2 < 10^3$ (Alexander & Hopman 2007, in prep.). The DFs are not exact power-laws, and the logarithmic slopes $p_M(x) = \mathrm{d}\log g_M/\mathrm{d}\log x$ depend somewhat on energy, especially near the boundaries. However, analysis of the results is considerably simplified by the fact that the values of $p_M(x)$ vary monotonically with μ_2 at all x, and so the order ranking of p_M for different models does not depend on the choice of x. Figure (9) shows p_L and p_H at $x = 10$, which corresponds to $r \sim 0.1$ pc in the GC. This choice samples $g_M(x)$ in a representative region, far from either boundaries at $x=0$ and $x_D = 10^4$, and translates to an observationally relevant region in the GC, which is close enough to the MBH to be nearly Keplerian, but still contains a large number of observed stars to allow meaningful statistics (cf Fig. 6).

Figure (9) shows that for $\mu_2 > 1$, the Fokker-Planck calculations recover the Bahcall-Wolf solution: $p_H \simeq 1/4$ irrespective of the mass ratio, and $p_L \simeq (1/4)(M_L/M_H)$. However, for $\mu_2 < 1$ there is a marked qualitative change in the nature of the solutions, as anticipated by the analysis in §3.2. The more the light stars dominate the population (the smaller μ_2), the more they approach the single population solution $p_L = 1/4$ (§3.1). The heavy stars settle to a much steeper cusp with $p_H > 1/4$. Figure (9) also shows the grid of models explored by Bahcall & Wolf (1977), which, while large, covers only the $\mu_2 > 1$ range. This explains why the strong segregation branch of the

† It is unlikely that real stellar system will have relaxational self-coupling parameters $\mu_2 \ll 0.1$. However, the study of such models is useful for understanding the mathematical properties of the solution.

solutions escaped their notice (their one model with $\mu_2 \simeq 0.6$ has a low mass ratio $M_H/M_L = 1.5$, where the two solution branches are not very different).

The $\mu_2 < 1$ models explored here follow the $p_M \propto M_\star$ relation noted by Bahcall & Wolf (1977) for the approximate mass-segregation solutions without a loss-cone term. Therefore, in those models where the limit $p_L \to 1/4$ is reached (for $M_H/M_L = 1.5$, 3), the heavy stars reach the asymptotic value $p_H \to (1/4)(M_H/M_L)$. It remains to be seen whether this result also holds for higher mass ratios, and for the full Fokker-Planck equation (Eq. 3.3) with the loss-cone term.

A realistic evolved stellar system, such as the GC, is expected to have a maximal mass ratio of at least $M_H/M_L = 10$ and $\mu_2 \simeq 0.15$ (Fig. 7). The mass-segregation calculations indicate that for these parameters the stellar BHs are expected to form an $\alpha_H \simeq 2.1$–2.2 cusp (Figs. 8, 9), significantly steeper than the $\alpha_H = 1.75$ predicted by the Bahcall-Wolf solution of moderate segregation. It is encouraging that this logarithmic slope is very close to that found in numerical simulations (Fig. 8) and that it is broadly consistent with what is needed to explain the observed trend in the stellar surface density distributions in the GC in terms of mass segregation (Fig. 6). In other systems the moderate segregation solution may apply. For example, if the globular cluster M15 contains an IMBH (e.g. Gerssen *et al.* 2002), then a tentative determination of its present-day mass function (Murphy *et al.* 1997) suggests a high relaxational self-coupling parameter, $\mu_2 \sim 40$ and a relatively shallow $\alpha = 7/4$ cusp of stellar BHs. Full-scale numeric simulations that are free of the restrictive assumptions of the analytic approach adopted here (Keplerian potential, fixed boundary conditions, approximate treatment of the loss-cone and a fixed 2-mass stellar population) are needed to verify and test these predictions in more detail.

Strong segregation will affect the cosmic rates of EMRI events. A detailed analysis of the anticipated change relative to the various discrepant published rate estimates depends on their specific assumptions (e.g. the assumed mass function, slope of the cusp, normalization of the stellar number density), and is outside the scope of this review.

4. Resonant relaxation

4.1. *Resonant relaxation dynamics*

The effect of 2-body relaxation on a test star is incoherent: the star experiences randomly oriented, uncorrelated perturbations from the ambient stars, and as a result its orbit deviates in a random-walk fashion from its original phase-space coordinates (in a stationary spherical smoothed potential where E and J would have been conserved in the continuum limit, $\Delta E \propto \sqrt{t}$ and $\Delta J \propto \sqrt{t}$ due to 2-body interactions). Resonant relaxation (RR) (Rauch & Tremaine 1996; Rauch & Ingalls 1998) is a form of accelerated relaxation of the orbital angular momentum, which occurs when approximate symmetries in the potential restrict the orbital evolution of the perturbing stars. This happens in the almost Keplerian potential near a MBH, where the orbits are approximately fixed ellipses (the potential of the enclosed stellar mass far from the MBH, or General Relativistic (GR) precession near the MBH, eventually leads to deviations from pure elliptical orbits), or in a non-Keplerian, but nearly spherically symmetric potential around a MBH, where the orbits approximately conserve their angular momentum and move on rosette-like planar orbits (the fluctuations in the potential due to stellar motions eventually lead to deviations from strictly planar orbits). As long as the symmetry is approximately conserved, on times shorter than the coherence timescale t_ω, the orbit of a test star with semi-major axis a experiences correlated (coherent) perturbations†, which can be described as a constant residual torque exerted by the superposed potentials of the $N_\star(< a)$ randomly oriented elliptical "mass wires" (in a Keplerian potential) or "mass annuli" (in a non-Keplerian spherical potential) that represent the

† RR is better described as "coherent relaxation". The term "resonant" refers to the equality of the radial and azimuthal orbital periods in a Keplerian potential, which results in closed ellipse orbits.

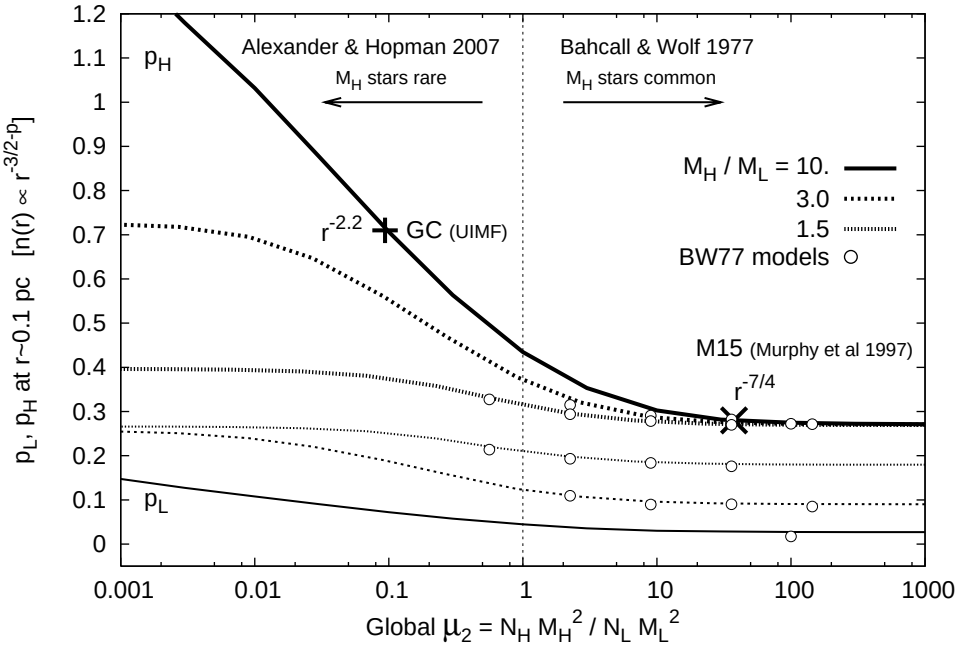

FIGURE 9. Fokker-Planck mass-segregation results. The logarithmic slopes p_H and p_L of the DFs of the heavy stars (thick lines) and light stars (narrow lines) , evaluated at ($r \sim 0.1$ pc in the GC), as function of the global relaxational self-coupling parameter μ_2, for mass ratios of $M_H/M_L = 1.5,\ 3,\ 10$ (Alexander & Hopman 2007, in prep.). The logarithmic slope of the stellar density of massive stars in the GC, assuming a universal IMF and continuous star formation history ($\mu_2 \sim 0.13$, Fig. 7, $\alpha_H = 3/2 + p_H \simeq 2.2$) is indicated by a cross on the left, and for globular cluster M15 (assuming it harbors an IMBH), on the right(estimated at $\mu_2 \sim 37$, based on the mass function model of Murphy *et al.* (1997), $\alpha_H \simeq 1.75$). The results for the models calculated by Bahcall & Wolf (1977) are indicated by circles.

orbitally-averaged mass distribution of individual perturbing stars. The magnitude of the residual torque is then $\dot{J} \sim N_\star^{1/2}(<a)GM_\star/a$ and the change in the angular momentum of the test star increases linearly with time, $\Delta J \sim \dot{J}t$ (for $t < t_w$). The orbital energy, on the other hand, remains unchanged, since the potential is constant.

RR in a Keplerian potential is called *scalar* RR since it changes both the magnitude and direction of **J**. Scalar RR can therefore change a circular orbit into an almost radial, MBH-approaching one. In contrast, RR in a non-Keplerian spherical potential is called *vector* RR since, for reasons of symmetry, it changes only the direction of **J**, but not its magnitude (Fig. 10). Vector RR can randomize the orbital orientations, but does not play a role in supplying stars to the loss-cone.

On timescales longer than the coherence time, the orbital orientations of the perturbing stars drift, and coherence is lost. the maximal change in angular momentum during the linear coherence time, $\Delta J_\omega \sim \dot{J}t_\omega$ then becomes the "mean free path" for a random walk in J-space, whose time-step is t_ω. On timescales longer than the coherence time, the angular momentum changes incoherently $\propto \sqrt{t}$, but much faster than it would have in the absence of RR. The energy is unaffected by RR and always evolves incoherently $\propto \sqrt{t}$ on the long non-resonant relaxation timescale (Fig. 11). The RR timescale T_{RR} is defined, like the incoherent 2-body relaxation timescale, as the time to change J by order J_c (Eqs. 1.1, 1.2), $T_{RR} \sim (J_c/\Delta J_\omega)^2\, t_\omega$, which can

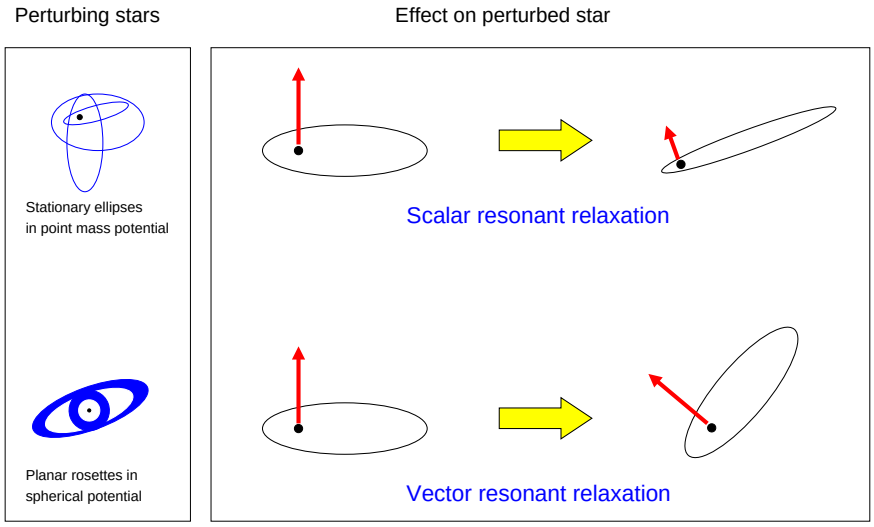

FIGURE 10. A sketch comparing the symmetries leading to scalar and vector RR. Top: The torques by fixed elliptical "mass wires" in a Keplerian potential lead to rapid changes in both the direction and magnitude of the orbital angular momentum of a test star. Bottom: The torques by fixed "mass annuli" in a non-Keplerian spherical potential lead to rapid changes in the direction, but not in the magnitude of the orbital angular momentum of a test star.

be expressed as (Hopman & Alexander 2006*a*)

$$T_{RR} = A^{\omega}_{RR}\frac{N_\star(<a)}{\mu^2(<a)}\frac{P^2(a)}{t_\omega} \simeq \frac{A^{\omega}_{RR}}{N_\star(<a)}\left(\frac{M_\bullet}{M_\star}\right)^2\frac{P^2(a)}{t_\omega}\,, \tag{4.1}$$

where μ is the relative enclosed enclosed stellar mass, $\mu = N_\star M_\star/\left(M_\bullet + N_\star M_\star\right)$, P is the radial orbital period, and the last approximate equality holds in the Keplerian regime. Here and below, the constants A^{ω}_{RR} are numerical factors of order unity that depend on the specifics of the coherence-limiting process, on the orbital characteristics of the test star, and probably also on the parameters of the stellar distribution. These constants are not well-determined at this time.

The coherence time depends on the symmetry assumed and on the process that breaks it. For a non-relativistic near-Keplerian potential, the limiting process is precession due to the potential of the distributed stellar mass†,

$$t_\omega = t_M \sim \frac{M_\bullet}{N_\star(<a)M_\star}P(a)\,. \tag{4.2}$$

Remarkably, the resulting RR timescale does not depend on $N_\star$. Close to the MBH is much shorter than the non-coherent 2-body relaxation timescale (here denoted for emphasis as T_{NR}),

$$T^{M}_{RR} = A^{M}_{RR}\frac{M_\bullet}{M_\star}P(a) \sim \frac{N_\star(<a)M_\star}{M_\bullet}T_{NR}\,. \tag{4.3}$$

Yet closer to the MBH, it is GR precession that limits the coherence,

$$t_\omega = t_{GR} = \frac{8}{3}\left(\frac{J}{J_{\rm LSO}}\right)^2 P(a)\,, \tag{4.4}$$

where $J_{\rm LSO} = 4GM_\bullet/c$ is the last stable orbit for $\epsilon \ll c^2$. The GR precession is prograde, while

† The enclosed stellar mass $N_\star M_\star$ changes the Keplerian period $P \propto M_\bullet^{-1/2}$ by $\Delta P/P = N_\star M_\star/2M_\bullet = \Delta\varphi/2\pi$. Identifying de-coherence with a phase drift $\Delta\varphi = \pi$ then implies $t_M \sim (\pi/\Delta\varphi)P$.

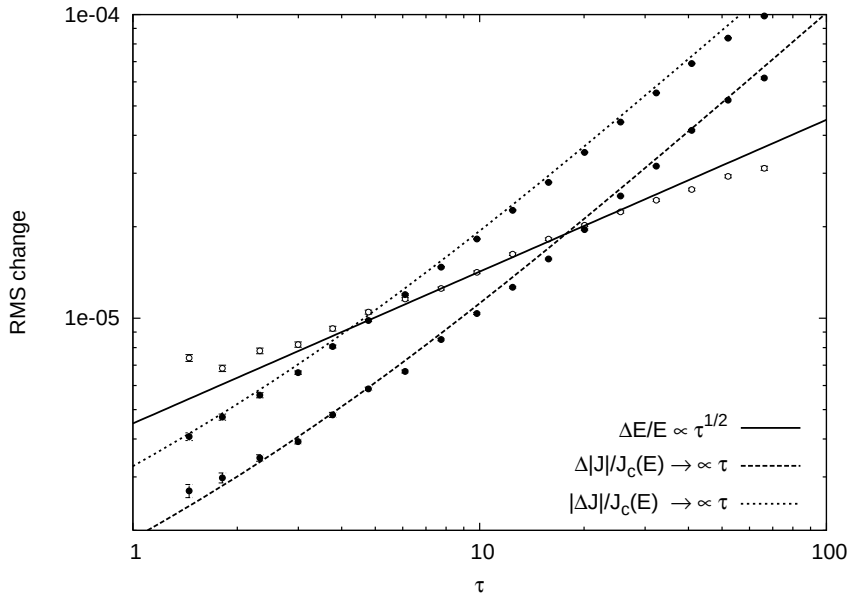

FIGURE 11. A correlation analysis of N-body simulations ($N=200$) showing the relaxation of energy and of scalar and vector angular momentum around a MBH in the Keplerian limit ($M_\star/M_\bullet = 3\times10^{-7}$) for a thermal population of stars, as function of the elapsed time-lag (Eilon, Kupi & Alexander, 2007, in prep.). The change in $\Delta E/E$, $\Delta J/J_c$ and $|\Delta\mathbf{J}|/J_c$ is plotted as function of the normalized time-lag $\tau=\Delta t/P$ in the range $1\le\tau\le100$. The mass precession coherence time of the system is $\tau_M = t_M/P \sim 1.7\times10^4$, and the potential fluctuation coherence time is $\tau_\phi = t_\phi/P \sim 1.2\times10^5$, so both scalar and vector RR are expected to grow linearly over the plotted range. More detailed analysis shows that the $\Delta J/J_c(E)$ is a function of both energy and angular momentum, which for $\tau\to0$ scales as $\sqrt{\tau}$, and for $1\ll\tau\ll\tau_w$ scales as τ, and that $|\Delta\mathbf{J}|/J_c$ is simply proportional to $\Delta J/J_c$. The correlation analysis is an efficient method for quantifying relaxation in N-body results (cf Rauch & Tremaine 1996, Fig. 1). The theoretical predictions for $\Delta J/J_c$ and $|\Delta\mathbf{J}|/J_c$ fit the numeric results very well. As expected, $\Delta E/E\propto\sqrt{\tau}$ at all time-lags.

that due to the distributed mass is retrograde, and so they may partially cancel each other. Their combined effect on the scalar RR timescale is

$$T^s_{RR} \simeq \frac{A^s_{RR}}{N_\star(<a)}\left(\frac{M_\bullet}{M_\star}\right)^2 P^2(a)\left|\frac{1}{t_M}-\frac{1}{t_{\rm GR}}\right| . \tag{4.5}$$

Since t_M increases with r, while $t_{\rm GR}$ decreases with r, scalar RR is fastest at some finite distance from the MBH, which typically coincides with $\sim r_{\rm crit}/2$ for LISA EMRI targets (Fig. 13).

Precession does not affect vector RR. The coherence in a non-Keplerian spherical potential is limited by the change in the total gravitational potential $\phi=\phi_\bullet+\phi_\star$ caused by the fluctuations in the stellar potential, $\phi_\star$, due to the realignment of the stars as they rotate by π on their orbits,

$$t_\omega = t_\phi = \frac{\phi}{\dot\phi_\star} \sim \frac{N_\star^{1/2}(<a)}{2\mu}P(a) \simeq \frac{M_\bullet}{2N_\star^{1/2}(<a)M_\star}P(a) , \tag{4.6}$$

where the last approximate equality holds in the Keplerian regime. The vector RR timescale is obtained by substituting t_ϕ in Eq. (4.1),

$$T^v_{RR} = 2A^v_{RR}\frac{N_\star^{1/2}(<a)}{\mu(<a)}P(a) \simeq 2A^v_{RR}\left(\frac{M_\bullet}{M_\star}\right)\frac{P(a)}{N_\star^{1/2}(<a)} . \tag{4.7}$$

Vector RR is much faster than scalar RR (Fig. 13).

4.2. *Resonant relaxation and EMRI rates*

The efficiency of scalar RR quickly decreases with distance from the MBH, since the coherence time falls as $M_\star(<r)/M_\bullet$ grows. At r_h, where $M_\star(<r_h)/M_\bullet \sim \mathcal{O}(1)$, scalar RR is almost completely quenched. Because $r_{\rm crit} \sim r_h$ for tidal disruption (Lightman & Shapiro 1977; §1.1), RR does not significantly enhance the tidal disruption rate (Rauch & Tremaine 1996). In contrast, $r_{\rm crit} \sim 0.01$ pc for EMRI events, where $M_\star(<r_{\rm crit})/M_\bullet \ll 1$ and T^s_{RR} is near its minimum. Scalar RR therefore dominates the dynamics of the loss-cone for GW EMRI events (Hopman & Alexander 2006*a*). Scalar RR accelerates the flow of stars in phase-space from large-J orbits to low-J orbits that approach the MBH and can lose orbital energy and angular momentum by the emission of GWs. However, if unchecked, RR would continue to rapidly drive the stars to plunging orbits that fall directly into the MBH. This is where GR precession is predicted to play an important role (Hopman & Alexander 2006*a*). Orbits with very small periapse, $r_p \sim {\rm few} \times r_s$, where GW emission becomes appreciable, are also orbits where the GR precession rate becomes large enough ($t_{\rm GR}$ becomes short enough) to quench RR, and allow the EMRI inspiral to proceed undisturbed. This subtle cancellation, which is critical for the observability of EMRI events, still has to be verified by direct simulations.

The effect of scalar RR can be included in an approximate way in the Fokker-Planck equation (Eq. 3.3) as an additional loss-cone term $R_{RR} \propto \chi g/T^s_{RR}$, where the efficiency factor χ parametrizes the uncertainties that enter through the various order-unity factors A^ω_{RR} (Eq. 4.1). Such calculations show that the poorly determined value of the efficiency can strongly affect the predicted EMRI rates (Fig. 12). As the efficiency rises, the EMRI rate first increases because stars are supplied faster to the loss-cone, but when the efficiency continues to rise the stars are drained so rapidly into the MBH, that the EMRI rates are strongly suppressed.

Rauch & Tremaine (1996) explored the efficiency of RR by a few small-scale N-body simulations, and noted a large variance around the derived mean efficiency. Here we use their mean efficiency as the reference point ($\chi = 1$), but consider also values smaller and larger. Figure (12) shows the GW inspiral rate and direct plunge rate as function of the unknown efficiency χ, relative to the no-RR case ($\chi = 0$), derived from Fokker-Planck calculations of a single mass population. The EMRI rate rises to ~ 8 times more than is expected without RR, peaking at $1 \lesssim \chi \lesssim 2$, but then falls rapidly to zero at $\chi \gtrsim 10$. The strong χ-dependence of the EMRI rates provides strong motivation to determine the RR efficiency and its dependence on the parameters of the system both numerically (Gürkan & Hopman 2007; Eilon, Kupi & Alexander 2007, in prep; Fig 11), and by direct observations of the only accessible system at present where RR effects may play a role—the stars around the Galactic MBH.

4.3. *Resonant relaxation and stellar populations in the GC*

The stellar population in the GC includes both young and old stars, and is composed of distinct sub-populations, each with its own kinematical properties (see Alexander 2005 for a review). As shown below, RR can naturally explain some of the systematic differences between the various dynamical components in the GC. Conversely, GC observations of these populations can then test the various assumptions and approximations that enter into analytic treatment of RR, and in particular constrain the poorly determined RR efficiency.

Figure (13) summarizes the typical distance scales and ages associated with these populations, and compares them with the various relaxation timescales. The calculation of the relaxation timescales are approximate since they assume a single mass population. The non-resonant 2-body relaxation timescale (Eq. 1.1) is roughly independent of radius in the GC, $T_{NR} \sim {\rm few} \times 10^9$ yr (assuming a mean stellar mass of $M_\star = 1\,M_\odot$; in a multi-mass system it is expected to decrease to $T_{NR} \sim 10^8$ yr in the inner 0.001 pc due to mass segregation, Hopman & Alexander 2006*b*). Because neither the RR efficiency, nor the mass function is known with confidence, the scalar RR timescale, T^s_{RR}, is shown for two different assumptions; $\chi M_\star = 1\,M_\odot$ and $\chi M_\star = 10\,M_\odot$.

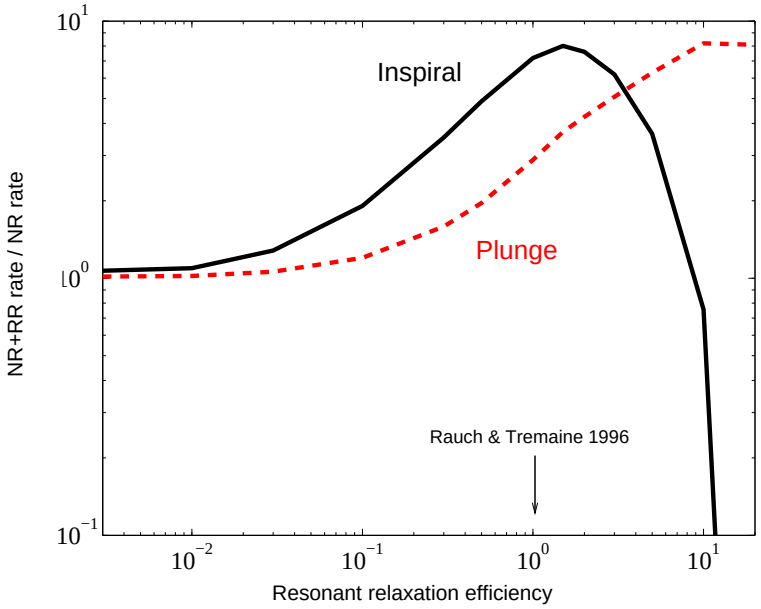

FIGURE 12. The relative rates of GW EMRI events and direct infall (plunge) events, as function of the unknown efficiency of RR, χ, normalized to $\chi=1$ for the values derived by Rauch & Tremaine (1996).

As discussed in §4.1, beyond $r\sim 0.1$ pc, $T^s_{RR}>T_{NR}$ due to mass precession, and the loss-cone replenishment is dominated by non-coherent relaxation. T^s_{RR} decreases toward the MBH, until it reaches a minimum, where it starts increasing again due to GR precession. The distance scale where T^s_{RR} is shortest happens to coincide with the volume $r\lesssim r_{\rm crit}$, where most GW EMRI sources are expected to lie and where $T^s_{RR}\ll T_{NR}$, so RR dominates EMRI loss-cone dynamics (§4.2). In contrast to scalar RR, the vector RR timescale T^v_{RR} (shown here for an assumed $\chi M_\star=1\,M_\odot$) decreases unquenched toward the MBH.

Dynamical populations and structures whose estimated age exceed these relaxation timescales must be relaxed. Those whose age cannot be determined, but whose lifespan exceeds the relaxation timescales may be affected, unless we are observing them at an atypical time soon after they were created. The youngest dynamical structure observed in the GC is the stellar disk (or possibly two non-aligned disks) (Levin & Beloborodov 2003; Genzel *et al.* 2003; Paumard *et al.* 2006), which is composed of ~ 50 young massive OB stars with an age of $t_\star\sim 6\pm 2$ Myr, on co-planar, co-rotating orbits that extend between ~ 0.04–0.5 pc. The inner edge of the disk is sharply defined and it coincides with the outer boundary of the S-stars cluster (§2.2). Figure (13) shows that the vector RR timescale equals the age of the stellar disk at its inner edge, and so is consistent with the spatial extent of the disk. Even if the S-stars were initially the inner part of the disk (this does not appear likely given that they are systematically lighter than the disk stars), vector RR would have efficiently randomized their orbital inclination. However, their measured high eccentricities (Eisenhauer *et al.* 2005; Ghez *et al.* 2005) would then be hard to explain. If instead, the S-stars are not-related to the disks, but were tidally captured around the MBH by 3-body exchange interactions (§2.3), then only their lifespan can be determined. Tidal capture leads to an extremely eccentric captured orbit (Eq. 2.2). Scalar RR could then randomize and decrease the eccentricities of at least a few of the older S-stars closer to the MBH. Vector and scalar RR could also explain why the old evolved giants (with progenitor masses of $M_\star\sim 2$–$8\,M_\odot$, Genzel *et al.* 1994) at $r\gtrsim 0.1$ pc appear dynamically relaxed (Genzel *et al.* 2000), in spite of the fact that their lifespans are shorter than the non-coherent relaxation time.

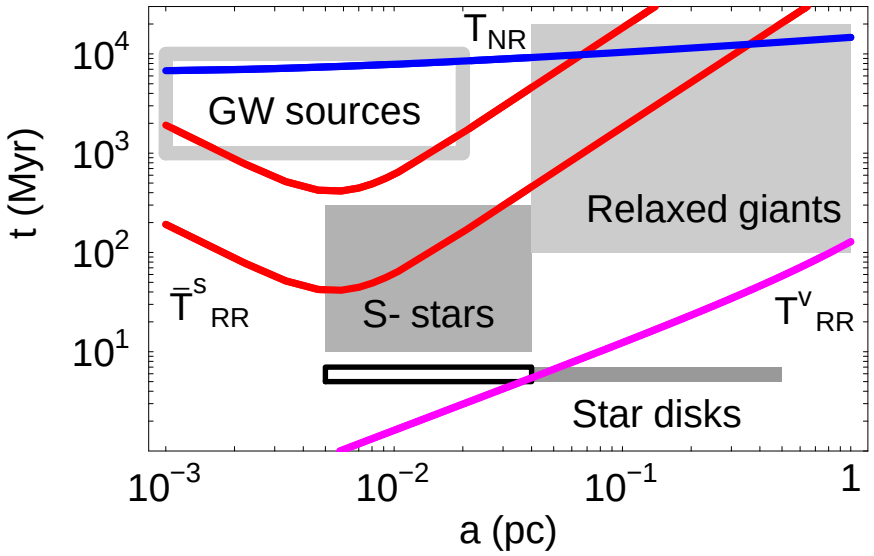

FIGURE 13. Evidence for resonant relaxation in the GC in the age .vs. distance from the MBH plane. The spatial extent and estimated age of the various dynamical sub-populations in the GC (shaded areas) is compared with the non-resonant 2-body relaxation timescale (top line, for assumed mean mass of $M_\star = 1\,M_\odot$) and with the scalar RR timescale (two curved lines, top one for $\chi M_\star = 1\,M_\odot$, bottom one for $\chi M_\star = 10\,M_\odot$) and vector RR timescale (bottom line, for $\chi M_\star = 1\,M_\odot$). The populations include the young stellar rings in the GC (filled rectangle in the bottom right); the S-stars, if they were born with the disks (open rectangle in the bottom left); the maximal lifespan of the S-stars (filled rectangle in the middle left); the dynamically relaxed old red giants (filled rectangle in the top right); and the reservoir of GW inspiral sources, where the age is roughly estimated by the progenitor's age or the time to sink to the center (open rectangle in the top left). Stellar components that are older than the various relaxation times must be randomized. (Hopman & Alexander 2006*a*, reproduced with permission from the *Astrophysical Journal*).

It should be noted that the effect of RR on the stellar density distribution is not expected to be large even quite close to the MBH ($r \lesssim 0.1$ pc), unless the efficiency χ is very high, because the RR-induced depletion of the DF at high energies is smoothed by the transformation from the DF to $n_\star(r)$ (Eq. 3.4) and by the contribution of unbound stars to the central density.

5. Summary

Relaxation processes play an important role in the GC, where the 2-body relaxation time is shorter than the age of the system and the stellar density is high. The scaling laws that follow from the $M_\bullet/\sigma$ relation imply that the same must hold for all galaxies with $M_\bullet \lesssim \mathrm{few} \times 10^7\,M_\odot$. Relaxation processes affect the distribution of stars and compact remnants, lead to close interactions between them and the MBH, and may be related to the unusual stellar populations that are observed in the GC. These are of relevance because of the very high quality stellar data coming from the GC, and because galactic nuclei with low-mass MBHs like the GC are expected to be important GW EMRI targets for the next generation of space borne GW detectors. In addition, efficient relaxation mechanisms that operate and can be studied in the GC may play a role even in galactic nuclei with high-mass MBHs, where 2-body relaxation is unimportant.

Three processes beyond minimal two-body relaxation were discussed here: accelerated loss-cone replenishment by MPs, strong mass-segregation in evolved populations, and rapid RR. Evidence was presented that these processes operate and may even dominate relaxation and its consequences in the GC: The S-stars and HVSs are consistent with relaxation by GMCs; there are hints for strong mass segregation in the central density suppression of the low-mass Red

Clump giants and in numeric simulations of the GC, and RR appears to play a role in the truncation of the stellar disks and the orbital randomization of the S-stars and the late type giants. There are also cosmic implications: MPs enable the efficient merger of binary MBHs, and boost the rates of white dwarf EMRIs captured near the MBH by tidal disruptions of stellar binaries. Strong segregation, and in particular RR can strongly affect the EMRI rates from stellar BHs.

The stellar dynamics laboratory in the GC holds great promise for future progress in understanding these mechanisms and their implications.

REFERENCES

ALEXANDER, T. 2005 Stellar processes near the massive black hole in the Galactic center [review article]. *Phys. Rep.* **419**, 65–142.

ALEXANDER, T. & HOPMAN, C. 2003 Orbital In-spiral into a Massive Black Hole in a Galactic Center. *ApJ* **590**, L29–L32.

ALEXANDER, T. & LIVIO, M. 2001 Tidal Scattering of Stars on Supermassive Black Holes in Galactic Centers. *ApJ* **560**, L143–L146.

ALEXANDER, T. & MORRIS, M. 2003 Squeezars: Tidally Powered Stars Orbiting a Massive Black Hole. *ApJ* **590**, L25–L28.

ALEXANDER, T. & STERNBERG, A. 1999 Near-Infrared Microlensing of Stars by the Supermassive Black Hole in the Galactic Center. *ApJ* **520**, 137–148.

AMARO-SEOANE, P., GAIR, J. R., FREITAG, M., MILLER, M. C., MANDEL, I., CUTLER, C. J. & BABAK, S. 2007 Astrophysics, detection and science applications of intermediate- and extreme mass-ratio inspirals. Submitted to Classical and Quantum Gravity (ArXiv:astro-ph/0703495).

BAHCALL, J. N. & WOLF, R. A. 1976 Star distribution around a massive black hole in a globular cluster. *ApJ* **209**, 214–232.

BAHCALL, J. N. & WOLF, R. A. 1977 The star distribution around a massive black hole in a globular cluster. II Unequal star masses. *ApJ* **216**, 883–907.

BAILEY, M. E. 1983 The structure and evolution of the solar system comet cloud. *MNRAS* **204**, 603–633.

BAUMGARDT, H., GUALANDRIS, A. & PORTEGIES ZWART, S. 2006 Ejection of hypervelocity stars from the Galactic Centre by intermediate-mass black holes. *MNRAS* **372**, 174–182.

BEGELMAN, M. C., BLANDFORD, R. D. & REES, M. J. 1980 Massive black hole binaries in active galactic nuclei. *Nature* **287**, 307–309.

BENDER, R. *et al.* 2005 HST STIS Spectroscopy of the Triple Nucleus of M31: Two Nested Disks in Keplerian Rotation around a Supermassive Black Hole. *ApJ* **631**, 280–300.

BERCZIK, P., MERRITT, D. & SPURZEM, R. 2005 Long-Term Evolution of Massive Black Hole Binaries. II. Binary Evolution in Low-Density Galaxies. *ApJ* **633**, 680–687.

BERCZIK, P., MERRITT, D., SPURZEM, R. & BISCHOF, H.-P. 2006 Efficient Merger of Binary Supermassive Black Holes in Nonaxisymmetric Galaxies. *ApJ* **642**, L21–L24.

BINNEY, J. & TREMAINE, S. 1987 *Galactic Dynamics*. Princeton, NJ: Princeton University Press.

BLAES, O., LEE, M. H. & SOCRATES, A. 2002 The Kozai Mechanism and the Evolution of Binary Supermassive Black Holes. *ApJ* **578**, 775–786.

BORISSOVA, J., IVANOV, V. D., MINNITI, D., GEISLER, D. & STEPHENS, A. W. 2005 Discovery of new Milky Way star cluster candidates in the 2MASS point source catalog. III. Follow-up observations of cluster candidates in the Galactic Center region. *A&A* **435**, 95–105.

BROMLEY, B. C., KENYON, S. J., GELLER, M. J., BARCIKOWSKI, E., BROWN, W. R. & KURTZ, M. J. 2006 Hypervelocity Stars: Predicting the Spectrum of Ejection Velocities. *ApJ* **653**, 1194–1202.

BROWN, W. R., GELLER, M. J., KENYON, S. J. & KURTZ, M. J. 2005 Discovery of an Unbound Hypervelocity Star in the Milky Way Halo. *ApJ* **622**, L33–L36.

BROWN, W. R., GELLER, M. J., KENYON, S. J. & KURTZ, M. J. 2006*a* A Successful Targeted Search for Hypervelocity Stars. *ApJ* **640**, L35–L38.

BROWN, W. R., GELLER, M. J., KENYON, S. J. & KURTZ, M. J. 2006*b* Hypervelocity Stars. I. The Spectroscopic Survey. *ApJ* **647**, 303–311.

CHRISTOPHER, M. H., SCOVILLE, N. Z., STOLOVY, S. R. & YUN, M. S. 2005 HCN and HCO^+ Observations of the Galactic Circumnuclear Disk. *ApJ* **622**, 346–365.

DOTTI, M., COLPI, M., HAARDT, F. & MAYER, L. 2007 Supermassive black hole binaries in gaseous and stellar circumnuclear discs: orbital dynamics and gas accretion. *MNRAS* pp. 582–+.

DUQUENNOY, A. & MAYOR, M. 1991 Multiplicity among solar-type stars in the solar neighbourhood. II - Distribution of the orbital elements in an unbiased sample. *A&A* **248**, 485–524.

EDELMANN, H., NAPIWOTZKI, R., HEBER, U., CHRISTLIEB, N. & REIMERS, D. 2005 HE 0437-5439: An Unbound Hypervelocity Main-Sequence B-Type Star. *ApJ* **634**, L181–L184.

EISENHAUER, F. *et al.* 2005 SINFONI in the Galactic Center: Young Stars and Infrared Flares in the Central Light-Month. *ApJ* **628**, 246–259.

ESCALA, A., LARSON, R. B., COPPI, P. S. & MARDONES, D. 2005 The Role of Gas in the Merging of Massive Black Holes in Galactic Nuclei. II. Black Hole Merging in a Nuclear Gas Disk. *ApJ* **630**, 152–166.

FERRARESE, L., CÔTÉ, P., JORDÁN, A., PENG, E. W., BLAKESLEE, J. P., PIATEK, S., MEI, S., MERRITT, D., MILOSAVLJEVIĆ, M., TONRY, J. L. & WEST, M. J. 2006 The ACS Virgo Cluster Survey. VI. Isophotal Analysis and the Structure of Early-Type Galaxies. *ApJS* **164**, 334–434.

FERRARESE, L. & MERRITT, D. 2000 A Fundamental Relation between Supermassive Black Holes and Their Host Galaxies. *ApJ* **539**, L9–L12.

FIGER, D. F., KIM, S. S., MORRIS, M., SERABYN, E., RICH, R. M. & MCLEAN, I. S. 1999 Hubble Space Telescope/NICMOS Observations of Massive Stellar Clusters near the Galactic Center. *ApJ* **525**, 750–758.

FIGER, D. F., RICH, R. M., KIM, S. S., MORRIS, M. & SERABYN, E. 2004 An Extended Star Formation History for the Galactic Center from Hubble Space Telescope NICMOS Observations. *ApJ* **601**, 319–339.

FRANK, J. & REES, M. J. 1976 Effects of massive central black holes on dense stellar systems. *MNRAS* **176**, 633–647.

FREITAG, M., AMARO-SEOANE, P. & KALOGERA, V. 2006 Stellar Remnants in Galactic Nuclei: Mass Segregation. *ApJ* **649**, 91–117.

FREITAG, M. & BENZ, W. 2002 A new Monte Carlo code for star cluster simulations. II. Central black hole and stellar collisions. *A&A* **394**, 345–374.

GEBHARDT, K. *et al.* 2000 A Relationship between Nuclear Black Hole Mass and Galaxy Velocity Dispersion. *ApJ* **539**, L13–L16.

GENZEL, R., HOLLENBACH, D. & TOWNES, C. H. 1994 The nucleus of our Galaxy. *Reports of Progress in Physics* **57**, 417–479.

GENZEL, R., PICHON, C., ECKART, A., GERHARD, O. E. & OTT, T. 2000 Stellar dynamics in the Galactic Centre: proper motions and anisotropy. *MNRAS* **317**, 348–374.

GENZEL, R. *et al.* 2003 The Stellar Cusp around the Supermassive Black Hole in the Galactic Center. *ApJ* **594**, 812–832.

GERHARD, O. E. & BINNEY, J. 1985 Triaxial galaxies containing massive black holes or central density cusps. *MNRAS* **216**, 467–502.

GERSSEN, J., VAN DER MAREL, R. P., GEBHARDT, K., GUHATHAKURTA, P., PETERSON, R. C. & PRYOR, C. 2002 Hubble Space Telescope Evidence for an Intermediate-Mass Black Hole in the Globular Cluster M15. II. Kinematic Analysis and Dynamical Modeling. *AJ* **124**, 3270–3288.

GHEZ, A. M., SALIM, S., HORNSTEIN, S. D., TANNER, A., LU, J. R., MORRIS, M., BECKLIN, E. E. & DUCHÊNE, G. 2005 Stellar Orbits around the Galactic Center Black Hole. *ApJ* **620**, 744–757.

GINSBURG, I. & LOEB, A. 2006 The fate of former companions to hypervelocity stars originating at the Galactic Centre. *MNRAS* **368**, 221–225.

GOULD, A. & QUILLEN, A. C. 2003 Sagittarius A* Companion S0-2: A Probe of Very High Mass Star Formation. *ApJ* **592**, 935–940.

GRAHAM, A. W. 2004 Core Depletion from Coalescing Supermassive Black Holes. *ApJ* **613**, L33–L36.

GUALANDRIS, A., PORTEGIES ZWART, S. & SIPIOR, M. S. 2005 Three-body encounters in the Galactic Centre: the origin of the hypervelocity star SDSS J090745.0+024507. *MNRAS* **363**, 223–228.

GÜRKAN, M. A. & HOPMAN, C. 2007 Resonant relaxation near a massive black hole: the dependence on eccentricity. Submitted to MNRAS (ArXiv:astro-ph/0704.2709).

GÜSTEN, R. & PHILIPP, S. D. 2004 Galactic Center Molecular Clouds. In *The Dense Interstellar Medium in Galaxies* (ed. S. Pfalzner, C. Kramer, C. Staubmeier & A. Heithausen), pp. 253–+.

HAARDT, F., SESANA, A. & MADAU, P. 2006 Hardening in a time-evolving stellar background: hypervelocity stars, orbital decay and prediction for LISA. *Memorie della Societa Astronomica Italiana* **77**, 653–+.

HILLS, J. G. 1981 Comet showers and the steady-state infall of comets from the Oort cloud. *AJ* **86**, 1730–1740.

HILLS, J. G. 1988 Hyper-velocity and tidal stars from binaries disrupted by a massive Galactic black hole. *Nature* **331**, 687–689.

HILLS, J. G. 1991 Computer simulations of encounters between massive black holes and binaries. *AJ* **102**, 704–715.

HIRSCH, H. A., HEBER, U., O'TOOLE, S. J. & BRESOLIN, F. 2005 US 708 - an unbound hyper-velocity subluminous O star. *A&A* **444**, L61–L64.

HOFFMAN, L. & LOEB, A. 2007 Dynamics of triple black hole systems in hierarchically merging massive galaxies. MNRAS in press (arXiv:astro-ph/0612517).

HOLLEY-BOCKELMANN, K. & SIGURDSSON, S. 2006 A Full Loss Cone For Triaxial Galaxies. Submitted to MNRAS (ArXiv:astro-ph/0601520).

HOPMAN, C. & ALEXANDER, T. 2005 The Orbital Statistics of Stellar Inspiral and Relaxation near a Massive Black Hole: Characterizing Gravitational Wave Sources. *ApJ* **629**, 362–372.

HOPMAN, C. & ALEXANDER, T. 2006*a* Resonant Relaxation near a Massive Black Hole: The Stellar Distribution and Gravitational Wave Sources. *ApJ* **645**, 1152–1163.

HOPMAN, C. & ALEXANDER, T. 2006*b* The Effect of Mass Segregation on Gravitational Wave Sources near Massive Black Holes. *ApJ* **645**, L133–L136.

HOPMAN, C., FREITAG, M. & LARSON, S. L. 2007 Gravitational wave bursts from the Galactic massive black hole. *MNRAS* **378**, 129–136.

HOPMAN, C., PORTEGIES ZWART, S. F. & ALEXANDER, T. 2004 Ultraluminous X-Ray Sources as Intermediate-Mass Black Holes Fed by Tidally Captured Stars. *ApJ* **604**, L101–L104.

IVANOV, P. B., PAPALOIZOU, J. C. B. & POLNAREV, A. G. 1999 The evolution of a supermassive binary caused by an accretion disc. *MNRAS* **307**, 79–90.

IWASAWA, M., FUNATO, Y. & MAKINO, J. 2006 Evolution of Massive Black Hole Triples. I. Equal-Mass Binary-Single Systems. *ApJ* **651**, 1059–1067.

KOBULNICKY, H. A., FRYER, C. L. & KIMINKI, D. C. 2006 A Fresh Look at the Binary Characteristics Among Massive Stars with Implications for Supernova and X-Ray Binary Rates. Submitted to ApJ (ArXiv:astro-ph/0605069).

KROUPA, P. 2001 On the variation of the initial mass function. *MNRAS* **322**, 231–246.

LEVI, M. 2006 Mass segregation in the Galactic center near the massive black hole. Master's thesis, Weizmann Institute of Science.

LEVIN, Y. 2006 Ejection of High-Velocity Stars from the Galactic Center by an Inspiraling Intermediate-Mass Black Hole. *ApJ* **653**, 1203–1209.

LEVIN, Y. 2007 Starbursts near supermassive black holes: young stars in the Galactic Centre, and gravitational waves in LISA band. *MNRAS* **374**, 515–524.

LEVIN, Y. & BELOBORODOV, A. M. 2003 Stellar Disk in the Galactic Center: A Remnant of a Dense Accretion Disk? *ApJ* **590**, L33–L36.

LEVIN, Y., WU, A. & THOMMES, E. 2005 Intermediate-Mass Black Hole(s) and Stellar Orbits in the Galactic Center. *ApJ* **635**, 341–348.

LIGHTMAN, A. P. & SHAPIRO, S. L. 1977 The distribution and consumption rate of stars around a massive, collapsed object. *ApJ* **211**, 244–262.

MAGORRIAN, J. & TREMAINE, S. 1999 Rates of tidal disruption of stars by massive central black holes. *MNRAS* **309**, 447–460.

MAKINO, J. & EBISUZAKI, T. 1994 Triple black holes in the cores of galaxies. *ApJ* **436**, 607–610.

MANESS, H. *et al.* 2007 Evidence for a Long-Standing Top-Heavy IMF in the Central Parsec of the Galaxy. ApJ in press.

MERRITT, D., MIKKOLA, S. & SZELL, A. 2007 Long-Term Evolution of Massive Black Hole Binaries. III. Binary Evolution in Collisional Nuclei. Submitted to ApJ (ArXiv:astro-ph/0705.2745).

MERRITT, D. & MILOSAVLJEVIĆ, M. 2005 Massive Black Hole Binary Evolution. *Living Reviews in Relativity* **8**, 8–+.

MERRITT, D. & POON, M. Y. 2004 Chaotic Loss Cones and Black Hole Fueling. *ApJ* **606**, 788–798.

MERRITT, D. & SZELL, A. 2006 Dynamical Cusp Regeneration. *ApJ* **648**, 890–899.

MILLER, G. E. & SCALO, J. M. 1979 The initial mass function and stellar birthrate in the solar neighborhood. *ApJS* **41**, 513–547.

MILLER, M. C., FREITAG, M., HAMILTON, D. P. & LAUBURG, V. M. 2005 Binary Encounters with Supermassive Black Holes: Zero-Eccentricity LISA Events. *ApJ* **631**, L117–L120.

MILOSAVLJEVIĆ, M., MERRITT, D., REST, A. & VAN DEN BOSCH, F. C. 2002 Galaxy cores as relics of black hole mergers. *MNRAS* **331**, L51–L55.

MIRALDA-ESCUDÉ, J. & GOULD, A. 2000 A Cluster of Black Holes at the Galactic Center. *ApJ* **545**, 847–853.

MURPHY, B. W., COHN, H. N., LUGGER, P. M. & DRUKIER, G. A. 1997 The Stellar Mass Function of the Globular Cluster M15. In *Bulletin of the American Astronomical Society*, *Bulletin of the American Astronomical Society*, vol. 29, pp. 1338–+.

NORMAN, C. & SILK, J. 1983 The dynamics and fueling of active nuclei. *ApJ* **266**, 502–515.

OKA, T., HASEGAWA, T., SATO, F., TSUBOI, M., MIYAZAKI, A. & SUGIMOTO, M. 2001 Statistical Properties of Molecular Clouds in the Galactic Center. *ApJ* **562**, 348–362.

PAUMARD, T. *et al.* 2006 The Two Young Star Disks in the Central Parsec of the Galaxy: Properties, Dynamics, and Formation. *ApJ* **643**, 1011–1035.

PERETS, H. B. & ALEXANDER, T. 2007 Massive perturbers and the efficient merger of binary massive black holes. Submitted to ApJ (ArXiv:astro-ph/0705.2123).

PERETS, H. B., HOPMAN, C. & ALEXANDER, T. 2007 Massive Perturber-driven Interactions between Stars and a Massive Black Hole. *ApJ* **656**, 709–720.

PETERS, P. C. 1964 Gravitational Radiation and the Motion of Two Point Masses. *Physical Review* **136**, 1224–1232.

POLNAREV, A. G. & REES, M. J. 1994 Binary black hole in a dense star cluster. *A&A* **283**, 301–312.

RAUCH, K. P. & INGALLS, B. 1998 Resonant tidal disruption in galactic nuclei. *MNRAS* **299**, 1231–1241.

RAUCH, K. P. & TREMAINE, S. 1996 Resonant relaxation in stellar systems. *New Astronomy* **1**, 149–170.

RAVINDRANATH, S., HO, L. C. & FILIPPENKO, A. V. 2002 Nuclear Cusps and Cores in Early-Type Galaxies as Relics of Binary Black Hole Mergers. *ApJ* **566**, 801–808.

RUBBO, L. J., HOLLEY-BOCKELMANN, K. & FINN, L. S. 2006 Event Rate for Extreme Mass Ratio Burst Signals in the Laser Interferometer Space Antenna Band. *ApJ* **649**, L25–L28.

SALPETER, E. E. 1955 The Luminosity Function and Stellar Evolution. *ApJ* **121**, 161–+.

SASLAW, W. C., VALTONEN, M. J. & AARSETH, S. J. 1974 The Gravitational Slingshot and the Structure of Extragalactic Radio Sources. *ApJ* **190**, 253–270.

SCHÖDEL, R. *et al.* 2007 The structure of the nuclear stellar cluster of the Milky Way. *A&A* **469**, 125–146.

SPITZER, L. J. & SCHWARZSCHILD, M. 1951 The Possible Influence of Interstellar Clouds on Stellar Velocities. *ApJ* **114**, 385–+.

SPITZER, L. J. & SCHWARZSCHILD, M. 1953 The Possible Influence of Interstellar Clouds on Stellar Velocities. II. *ApJ* **118**, 106–+.

SYER, D. & ULMER, A. 1999 Tidal disruption rates of stars in observed galaxies. *MNRAS* **306**, 35–42.

WANG, J. & MERRITT, D. 2004 Revised Rates of Stellar Disruption in Galactic Nuclei. *ApJ* **600**, 149–161.

WILLEMS, B. & KOLB, U. 2004 Detached white dwarf main-sequence star binaries. *A&A* **419**, 1057–1076.

YOUNG, P. J. 1977 The black tide model of QSOs. II - Destruction in an isothermal sphere. *ApJ* **215**, 36–52.

YU, Q. 2002 Evolution of massive binary black holes. *MNRAS* **331**, 935–958.

YU, Q. & TREMAINE, S. 2003 Ejection of Hypervelocity Stars by the (Binary) Black Hole in the Galactic Center. *ApJ* **599**, 1129–1138.

ZHAO, H., HAEHNELT, M. G. & REES, M. J. 2002 Feeding black holes at galactic centres by capture from isothermal cusps. *New Astronomy* **7**, 385–394.

ZIER, C. 2006 Merging of a massive binary due to ejection of bound stars. *MNRAS* pp. L67+.